iScience

CellPress
OPEN ACCESS

Article

Cocaine-regulated trafficking of dopamine transporters in cultured neurons revealed by a pH sensitive reporter

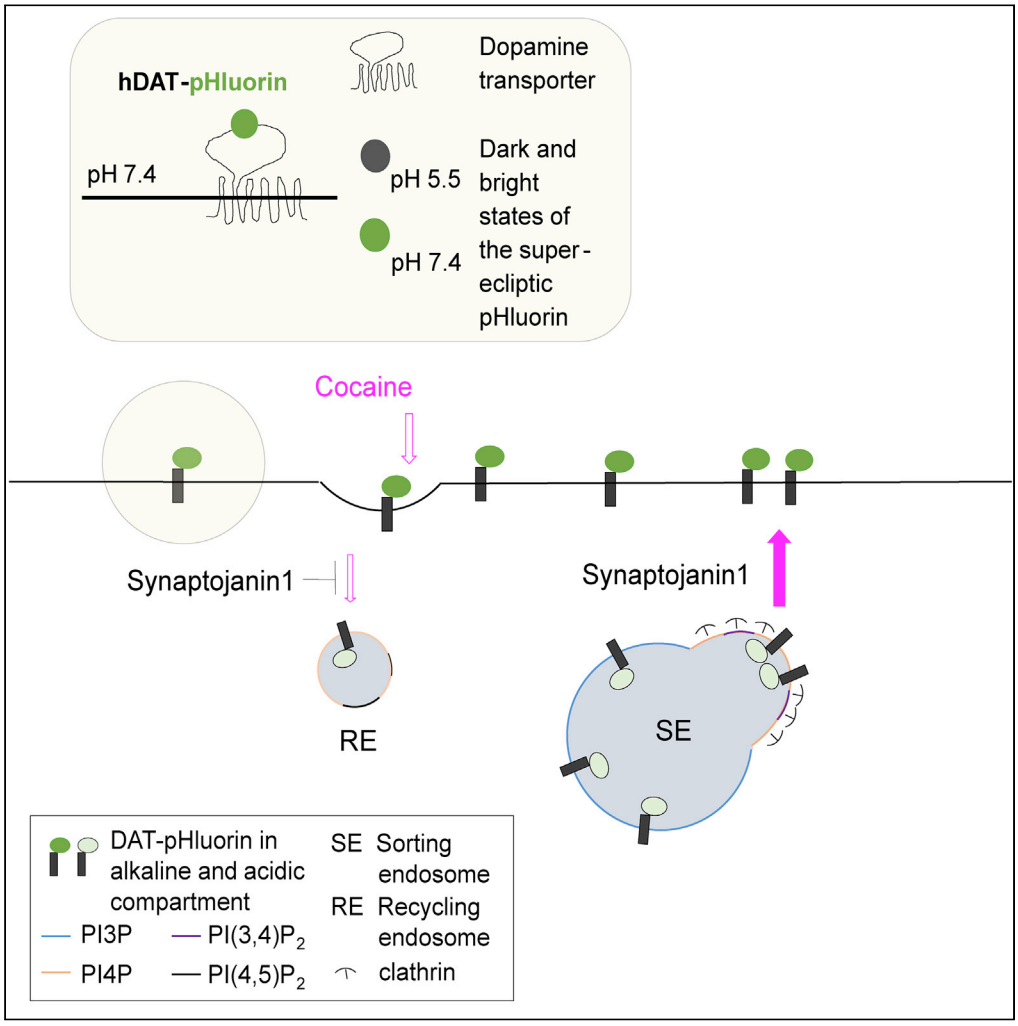

Jacqueline Saenz, Oscar Yao, Elnaz Khezerlou, ..., David J. Barker, Emanuel DiCicco-Bloom, Ping-Yue Pan

pingyue.pan@rutgers.edu

Highlights

DAT-pHluorin is engineered for studying dopamine transporter trafficking

DAT is predominantly localized to the plasma membrane in the axons

Cocaine induces a transient internalization of DAT followed by reinsertion

Synaptojanin1 regulates the cocaine-induced DAT trafficking

Saenz et al., iScience 26, 105782
January 20, 2023
https://doi.org/10.1016/j.isci.2022.105782

iScience

CellPress
OPEN ACCESS

Article

Cocaine-regulated trafficking of dopamine transporters in cultured neurons revealed by a pH sensitive reporter

Jacqueline Saenz,[1,2] Oscar Yao,[1] Elnaz Khezerlou,[1] Meha Aggarwal,[1] Xiaofeng Zhou,[3] David J. Barker,[4] Emanuel DiCicco-Bloom,[3] and Ping-Yue Pan[1,5,*]

SUMMARY

Cocaine acts by inhibiting plasma membrane dopamine transporter (DAT) function and altering its surface expression. The precise manner and mechanism by which cocaine regulates DAT trafficking, especially at neuronal processes, are poorly understood. In this study, we engineered and validated the use of DAT-pHluorin for studying DAT localization and its dynamic trafficking at neuronal processes of cultured mouse midbrain neurons. We demonstrate that unlike neuronal soma and dendrites, which contain a majority of the DATs in weakly acidic intracellular compartments, axonal DATs at both shafts and boutons are primarily (75%) localized to the plasma membrane, whereas large varicosities contain abundant intracellular DAT within acidic intracellular structures. We also demonstrate that cocaine exposure leads to a Synaptojanin1-sensitive DAT internalization process followed by membrane reinsertion that lasts for days. Thus, our study reveals the previously unknown dynamics and molecular regulation for cocaine-regulated DAT trafficking in neuronal processes.

INTRODUCTION

Dopamine (DA) signaling regulates a multitude of brain functions including motor coordination and reward processing. DA reuptake from the extracellular space into the cytosol by the plasma membrane dopamine transporter (DAT) is the primary mechanism for terminating DA signaling in the brain. Lack of DAT expression results in increased extracellular DA and hyperactive locomotion in the knockout mice.[1] Importantly, many psychoactive substances, such as cocaine and amphetamine (AMPH), directly or indirectly target plasma membrane DAT. In addition to acting to increase extracellular levels of DA, these substances are also known to impact DAT trafficking and plasma membrane expression.[2–6] The potency of these psychoactive substances in altering DA signaling is highly dependent on the amount of surface DAT expression, however, our understanding on the dynamic trafficking and molecular regulation of DAT, especially in neuronal processes, is poorly understood.

The lack of understanding largely reflects a lack of molecular tools to examine the dynamic trafficking of DAT in small neuronal structures like the axons and presynaptic terminals. Current understanding of DAT trafficking is largely based on studies of heterologous cells and isolated synaptosomes. The most commonly used research strategies to examine the surface DAT include (1) biotinylation assays, which has poor temporal resolution; (2) radioactive binding/uptake assays, which entangles DAT localization with function; and (3) imaging studies using fluorescent proteins-tagged DATs or fluorescent DAT ligands,[7,8] which exhibit limited spatial resolution for neuronal processes. Complex regulatory mechanisms have been proposed for DAT in different cell systems using different methods. For example, the constitutive DAT recycling can be regulated through a protein kinase C (PKC)-dependent[9] or independent manner.[10] AMPH was shown in most studies to induce DAT internalization via RhoA and TAAR1 signaling[11–13]; however, AMPH-induced delivery of DAT to the plasma membrane has also been reported.[14] Cocaine was found in various studies to block DAT internalization and to increase its surface expression.[15–20] Of interest, however, the mechanisms underlying cocaine-regulated DAT trafficking remain elusive, likely because of its inhibitory role on DAT function that hinders the use of many conventional methods. An earlier study by Sorkin et al. further suggested that neuronal DAT trafficking might be regulated by different mechanisms than what we learned from heterologous cells.[21]

[1]Rutgers University Robert Wood Johnson Medical School, Department of Neuroscience and Cell Biology, 675 Hoes Lane West, Piscataway, NJ 08854, USA

[2]Rutgers Graduate School of Biomedical Sciences, Molecular Biosciences Graduate Program, Piscataway, NJ 08854, USA

[3]Rutgers University Robert Wood Johnson Medical School, Department of Neuroscience and Cell Biology, 683 Hoes Lane West, Piscataway, NJ 08854, USA

[4]Rutgers, The State University of New Jersey, Department of Psychology, 152 Frelinghuysen Road, Piscataway, NJ 08854, USA

[5]Lead contact

*Correspondence: pingyue.pan@rutgers.edu

https://doi.org/10.1016/j.isci.2022.105782

To better reveal and understand DAT trafficking in neurons, we sought to develop a genetically encoded optical reporter. The pH sensitive "pHluorin" is a variant of green fluorescent proteins (GFP) that fluoresces on deprotonation.[22] pHluorin-based assays are best known for analyzing synaptic vesicle recycling when pHluorin is tagged to synaptic vesicle proteins, such as vesicle associated membrane protein 2/VAMP2 (synaptopHluorin),[22,23] vesicular glutamate transporter 1/VGlut1,[24,25] and vesicular monoamine transporter 2/vMAT2.[26,27] In addition, pHluorin has also been successfully engineered into plasma membrane cargo proteins, such as AMPA receptors,[28,29] transferrin receptors,[30] mu-opioid receptors[31,32] and glucose transporter 4 (GluT4)[33,34] for analyzing their endosomal trafficking. We have now engineered pHluorin into the second exofacial loop of human DAT. By expressing DAT-pHluorin in cultured midbrain (MB) neurons, we turn DAT trafficking events at nano/micrometer scales to measurable changes in fluorescence using a conventional wide-field microscope. We demonstrate that 75% of axonal DAT is on the plasma membrane, with most intracellular DAT found in the varicosities. Moreover, we reveal the dynamic trafficking of DAT to the axonal surface in response to cocaine, which lasts for up to 4 days. The surface trafficking of DAT is regulated by synaptojanin1, a phosphoinositol phosphatase that was previously known to regulate synaptic vesicle recycling[35–41] and autophagy.[41–43] Thus, our study using the newly engineered DAT optical reporter reveals, for the first time, cocaine-regulated DAT trafficking in neuronal processes.

RESULTS

Engineering and characterization of a pH sensitive DAT reporter

DAT belongs to the family of Na^+/Cl^- dependent neurotransmitter transporters[44] and contains 12 transmembrane domains. An extensive body of work has shown that DAT substrates, such as DA, AMPH or cocaine, can induce DAT trafficking.[2,3] To engineer a DAT reporter suited for reporting physiologically relevant DAT endosomal trafficking, our strategy is to insert pHluorin while not, or minimally, disrupting its endogenous functions in substrate binding. Among the six extracellular loops of human DAT cDNA, the second loop was selected due to the optimal length of the loop that provides flexibility for accommodating a tag protein (Figure 1A). Flexible linkers were inserted on both ends of pHluorin to introduce additional flexibility for the proper folding of the reporter. pHluorin was inserted at multiple sites, T173/E174, P194/G195, G199/S201, G209/T210, R219/G220 outside the known functional sites of DAT.[45–48] Although some insertion sites (T173/E174, G209/T210) resulted in poor expression of the transgene in the initial screen, little difference was observed for the remaining versions of DAT-pHluorin (DAT-pH) in their overall expression patterns (data not shown). We thus proceeded to further validate the DAT-pH at the P194/G195 insertion site, where an HA epitope was inserted in earlier studies.[49,50]

When expressed in cultured MB neurons, we found that DAT-pH exhibited homogeneous cell body expression similar to endogenous DAT, and it was recognized by an anti-DAT antibody (Figure 1B). DAT-pH was targeted to express in distal axons in both DAergic and non-DAergic neurons in the culture (Figure 1C). In the past, fluorescent proteins such as YFP have been tagged to the N-terminus of DAT to track DAT trafficking in heterologous cells. We next examined the expression of DAT-pH in N2a cells by comparing to other tagged/fluorescent DAT reporters (Figure 1D). Unlike the N-terminally tagged DATs, which often exhibit supraphysiological levels of plasma membrane localization,[46,48]DAT-pH expression was predominantly intracellular, but exhibited perfect colocalization when coexpressed with DAT-HA (Figure 1D). To determine if a fraction of DAT-pH was indeed targeted to express on the plasma membrane we performed the ^{3}H-DA uptake assay. N2a cells transfected with DAT-pH exhibited a near 40-fold increase in ^{3}H-DA uptake. Although it was only a fraction of the ^{3}H-DA uptake in YFP-DAT expressing cells, DAT-pH in N2a cells performed similarly compared to the endogenous transporter activity measured in SH-SY5Y cells (Figure 1E). A 60-min cocaine exposure inhibited DA uptake for N2a cells expressing DAT-pH by 90%, similar to the cocaine's effect on endogenous transporters in SH-SY5Y cells (Figure 1F). These data further suggested that pHluorin insertion did not block the essential substrate binding sites on DAT.

As a reporter gene that was designed to retain endogenous functions, an important concern is the potential unregulated expression that leads to altered intracellular signaling. An earlier study by Ryan et al. showed that only 1–2 copies of VGlut1-pHluorin (equivalent to a 10–20% overexpression) expression on the synaptic vesicle was sufficient to serve as a working sensor.[51] Using immunofluorescence labeling of DAT, we found that DA neurons expressing DAT-pH exhibited similar levels of overall DAT expression compared to the untransfected neurons (Figures S1A and S1B). We then analyzed DAT surface expression in transfected and untransfected neurons using a fluorescent cocaine analogue, JHC1-64[7,8,52] following

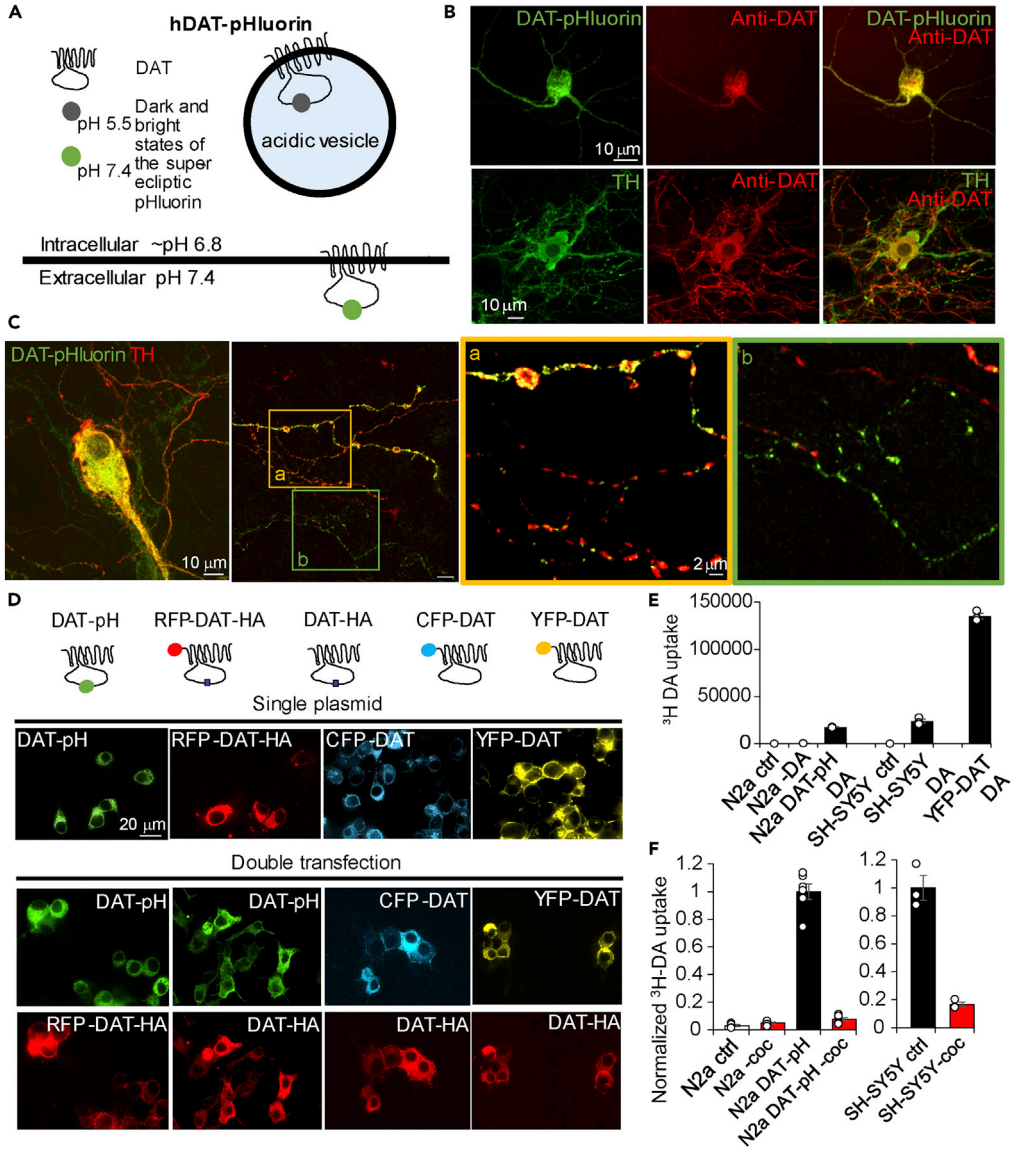

Figure 1. Engineering and validation of a pH sensitive DAT reporter

(A) Working hypothesis of the pH sensitive DAT reporter. The pH sensitive GFP variant, pHluorin, was inserted between the 194 Proline and 195 Glycine of the second exofacial loop of human DAT. This design allows DAT-pHluorin to fluoresce at its brightest when inserted onto the plasma membrane to face a neutral (pH 7.4) extracellular medium; and quenches when endocytosed to face an acidic endocytic compartment.

(B) Top, cultured MB neuron expressing DAT-pH and immunolabeled with anti-GFP (green) and anti-DAT antibodies (red). Bottom, cultured MB neuron immunolabeled with anti-TH (green) and anti-DAT (red) reveals the endogenous protein.

(C) Cultured MB dopamine neurons expressing DAT-pH and immunolabeled with anti-GFP (green) and anti-TH (red) antibodies. From left to right are the cell body, distal axon, and the enlarged view of the two cropped areas of the distal axons containing TH-positive (a) and TH-negative (b) axons.

(D) Comparison of the expression and co-expression patterns of DAT-pHluorin (DAT-pH) and other versions of tagged-DAT in N2a cells. Top, illustrations of the molecular structure and location of the tag for all DAT reporters. Representative images selected from N = 3 repeats.

(E) 3H-DA uptake for N2a cells, N2a cells expressing DAT-pHluorin, SH-SY5Y cells and N2a cells expressing YFP-DAT. N = 3 replicates.

(F) Bar graphs of normalized 3H-DA uptake for SH-SY5Y cells, N2a cells and N2a cells expressing DAT-pHluorin in response to cocaine (10 μM). N = 6 replicates for N2a cells and N = 3 for SH-SY5Y cells. See also Figure S1.

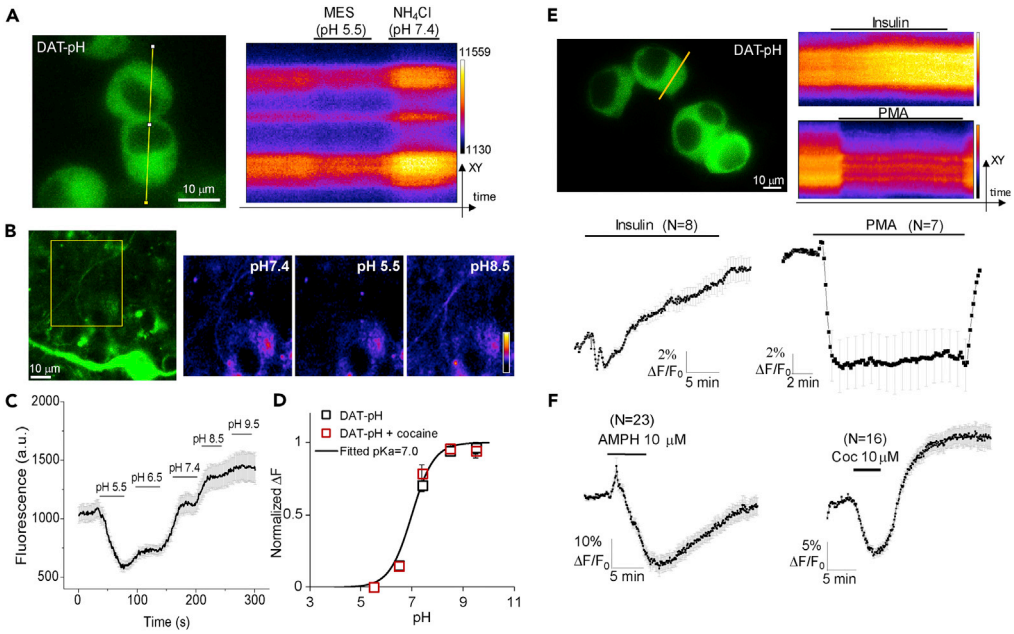

Figure 2. DAT-pHluorin exhibits reliable pH sensitivity and ligand regulated trafficking

(A) N2a cells expressing DAT-pH were perfused with a pH 5.5 MES solution followed by a pH 7.4 NH_4Cl solution. Right, kymographs were generated from the yellow line of the image on the left.

(B) Representative MB neuron expressing DAT-pH and axons (yellow boxed region) were selected for analyzing the pKa. Image intensities were adjusted to visualize the axon. Cell body fluorescence was not saturated at the camera. Right panels are the representative axon with color coding for DAT-pH immunofluorescence taken at different time points during a sequential perfusion of pH-fixed solutions shown in C.

(C) Representative DAT-pH signal when perfused with MES buffered saline at pH5.5 and 5.6, NH_4Cl solution at 7.4, and Bicine buffered saline at pH8.5 and 9.5. Error bars are from standard errors of 31 regions of interests along the axon of one neuron.

(D) Summary of normalized changes in DAT-pH responses in (C) from 4 axons at rest (black symbols) and 5 axons after the repeated cocaine treatment (red symbols). Black line represents the fitted change in fluorescence assuming pKa = 7.0.

(E) N2a cells expressing DAT-pH and DAT-HA were perfused with Tyrode's solution containing insulin (20 μM) or PMA (1 μM) in separate imaging trials. Kymographs were generated from the yellow lines in the top left panel and the corresponding fluorescence signals of the cells were presented at the bottom. N = cell number, which is indicated next to the trace. Data is represented as mean ± SEM Similar responses were verified in three separate experiments.

(F) Averaged responses from N2a cells expressing DAT-pH and DAT-HA perfused with Tyrode's solution containing amphetamine/AMPH (10 μM, 5 min) or cocaine/coc (10 μM, 5 min). N = cell number. Data is represented as mean ± SEM from two independent cultures. See also Figure S2.

a validation study conducted in N2a cells (Figures S1C and S1D). We showed that JHC1-64 can bind to DAT-pH in non-DAergic neurons (Figure S1E). Expressing DAT-pH did not lead to an increase in JHC dye binding either at the cell body or the axons (Figures S1F and S1G). The reduced fluorescence at the axons could be because of reduced binding affinity for DAT-pH.

We next examined other functional properties of DAT-pH as a viable reporter. Perfusion of a pH 5.5 MES (2-(N-morpholino)ethanesulfonic acid) solution quenched DAT-pH fluorescence whereas a pH 7.4 NH_4Cl solution revealed its peak fluorescence at the cell body (Figure 2A). To determine if pHluorin insertion in the functional DAT molecule maintains its original pH sensitivity (estimated pKa ~7.1 in synaptopHluorin,[23] we measured the pKa of DAT-pH in the axons of MB neurons by sequentially perfusing a series of pH-fixed solutions following a previously reported protocol[23](Figures 2B and 2C). We found the best fitted pKa to be 7.0 for DAT-pH in MB neurons at rest, and that cocaine (10 μM for 4 days) treatment did not alter the pH sensitivity of the reporter (Figure 2D). Moreover, we examined if DAT-pH exhibits agonist-regulated trafficking. DAT has been shown in earlier studies to internalize on PKC activation,[46,53] and insulin was able to increase DAT surface expression via activation of the PI3K pathway.[54] Consistently, DAT-pH exhibited a time-locked insulin-induced increase in fluorescence and a PMA (phorbol myristate acetate)-induced decrease in fluorescence (Figure 2E), suggesting that the new reporter is responsive to PI3K and PKC

regulated trafficking. We then examined psychostimulants including AMPH and cocaine. A brief AMPH (10 μM) perfusion led to a robust decrease of the fluorescence, which returned to baseline on washout (Figure 2Fleft). Of interest, cocaine (10 μM) perfusion also induced a transient reduction of the DAT-pH signal, suggesting DAT internalization, which was followed by fast reversal and an increase of fluorescence within a few minutes (Figure 2Fright). Cocaine-induced DAT internalization in such timescale was not reported previously. To verify that the transient reduction of DAT-pH signal was indeed because of loss of surface DAT rather than a change in fluorescence because of conformational changes (such as oligomerization) of the reporter,[19] we performed surface staining in non-permeabilized cells following a 5-min cocaine (10 μM) incubation (Figures S2A and S2B). Our analysis suggested significant reduction of DAT surface fraction in cocaine treated cells (Figure S2B). Moreover, we did not observe major changes in the relative abundance of monomer, dimer and oligomers of the DAT-pH reporter following a 5-min or 10-min treatment of cocaine (10 μM) (Figure S2C).

Taken together, our analyses using complementary methods suggest that DAT-pH is a viable reporter for analyzing DAT trafficking in neurons.

Majority of axonal DAT is on the plasma membrane

We next transfected DAT-pH in cultured mouse midbrain neurons. By bath perfusing MES (pH 5.5) and NH_4Cl (pH 7.4) solutions, we were able to extract an MES response that represents the surface pool of DAT and an NH_4Cl response that represents intracellular DAT (Figures 3A, 3B, and S3A). In the cell body and proximal dendrites of the neuron, both surface and intracellular DATs were observed (Figures 3A–3C). Of interest, the intracellular DAT (NH_4Cl response) in majority of the axons (identified by their substantially thinner appearance) was either absent or significantly smaller compared to that from the dendrites and cell body (Figures 3B and 3C). In parallel, the axonal MES response is substantially larger compared to the cell bodies and dendrites (Figures 3B and S3B). To exclude the possibility of quenching intracellular DAT by MES (Figure S3C), we performed surface labeling of pHluorin using an anti-GFP antibody without permeabilizing the cell (Figures S3C and S3D). Our analysis revealed the highest ratio for the surface to intracellular labeling of pHluorin in the axons and the lowest ratio at the cell body Figure S3E), further suggesting a negligible contribution from the membrane permeability concerns of MES. To determine if DAT-pH yields different responses in DAergic versus non-DAergic neurons from the MB culture, we performed *post hoc* analysis based on tyrosine hydroxylase (TH) immunoreactivity of the neuron analyzed. Across four independent batches of the MB cultures, we did not observe significant differences in either the MES or NH_4Cl responses (Figure S4A).

The dynamic range of DAT-pH response is determined by the acidity of the intracellular structure that it is delivered to. To more accurately determine the surface DAT fraction in each neuronal compartment and the vesicular pH of the DAT-pH in that compartment, we used the Henderson-Hasselbalch equation with the fitted DAT-pH pKa of 7.0 (Figures 2B–2D), following previously published protocols (Figure 3D, see STAR Methods).[33,51] We report that neuronal cell body and dendrites contain 23.49 $\pm$ 1.75% (N = 37) and 35.64 $\pm$ 2.68% (N = 35) of surface DAT, respectively, whereas axonal DATs are primarily localized to the plasma membrane (73.1 $\pm$ 2.38%, N = 41) (Figure 3E). On average, DAT-containing vesicles are modestly but significantly more acidic in the axons (pH = 6.85 $\pm$ 0.014) compared to those in the cell body (pH = 6.94 $\pm$ 0.017) and dendrites (pH = 6.94 $\pm$ 0.022) (Figure 3F).

Large varicosities are distinct axonal sites that contain DAT in acidic intracellular organelles

The relative distribution of intracellular versus surface DAT at rest in different subcellular compartments of the neuron is reflective of constitutive DAT recycling.[9,48] In all axonal structures examined, a fraction of these exhibited a relatively large NH_4Cl response (Figure S3B), suggesting that parts of the axons might be subjected to active DAT internalization. However, it remains unclear whether DAT is internalized at random positions along the axon, or if there are designated structures that support DAT turnover. To address this question, we examined three different structures in the axon: (1) Synaptic boutons, which are active sites for synaptic vesicle recycling and exhibit punctate staining for synapsin (Figure 4A); (2) axonal shafts, which exhibit diffuse synapsin staining; and (3) large varicosities that often exhibit DAT-pH outlining at rest (Figure 4B) but weak or diffuse synapsin staining. These varicosities, although not observed in all axons, are not uncommon for MB neurons. They have been previously reported to be potential axonal branching points[55] and are presently viewed to be highly relevant in neural injury and neurodegeneration.[56–58] We found that only varicosities, but not axonal shafts or boutons exhibited a robust NH_4Cl

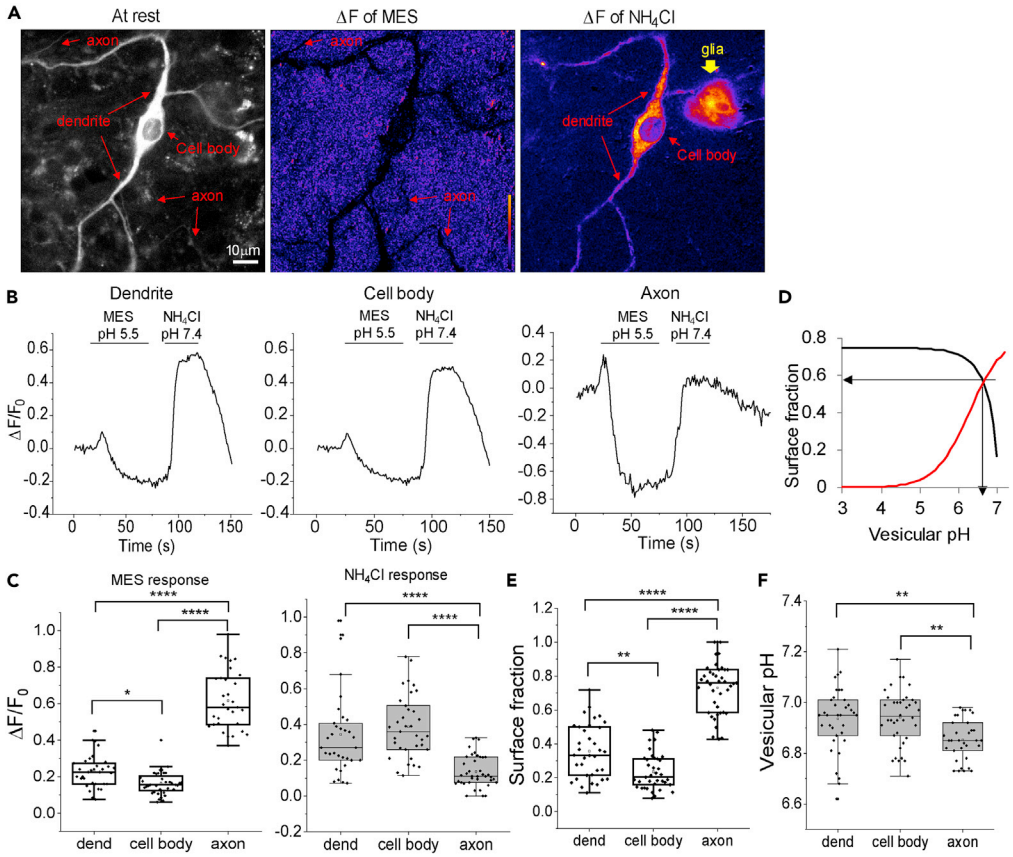

Figure 3. Majority of axonal DAT is on the plasma membrane

(A) Representative imaging field containing a cultured midbrain neuron and a neighboring glia expressing DAT-pHluorin. From left to right: fluorescent image at rest in gray scale, ΔF image of the negative response to the MES solution perfusion and ΔF image of the positive response to the NH4Cl solution perfusion. Arrows point to the cell body, neurites, and the glial cell, which were visible at different stages.

(B) Representative DAT-pHluorin signals measured from the dendrite, cell body and axon during a sequential MES and NH4Cl perfusion experiment.

(C)Box and whisker charts for the ΔF/F0 of the MES and NH4Cl responses measured at different compartments of the midbrain neuron. Each data point represents an averaged response from one cell across multiple trials. N = 33 for dendrites, N = 36 for cell bodies and N = 31 for axons. F = 159.67, p = 2.06E-31, one-way ANOVA for MES responses. ****p = 0.0000 comparing axons versus dendrites and axons versus cell bodies; *p = 0.044 comparing dendrites versus cell bodies, Bonferroni *post hoc* following one-way ANOVA. F = 22.56, p = 7.29E-9, one-way ANOVA for NH_4Cl responses. ****p < 1.00E-5 comparing axons versus dendrites; ****p < 1.00E-7 axons versus cell bodies; p = 0.90 comparing dendrites versus cell bodies, Bonferroni *post hoc* following one-way ANOVA. Data from four batches of cultures.

(D) Illustration for the calculation of surface fraction and vesicular pH based on the $\Delta F/F_0$ measurements obtained in (B) using the Henderson-Hasselbalch equation (see STAR Methods).

(E and F) Box and whisker charts summarizing the surface fraction (E) and vesicular pH (F) of DAT-pH in different cellular compartments. F = 131.72, p = 6.37E-30, one-way ANOVA for surface fraction. ****p = 0.0000 comparing axons versus dendrites and axons versus cell bodies; **p = 0.0012 comparing dendrites versus cell bodies, Bonferroni *post hoc* following one-way ANOVA. F = 7.14, p = 0.0013, one-way ANOVA for vesicular pH. **p = 0.0063 comparing axons versus dendrites; **p = 0.0026 comparing axons versus cell bodies; p = 1.00 comparing dendrites versus cell bodies, Bonferroni *post hoc* following one-way ANOVA. See also Figures S3 and S4.

response (Figures 4B and 4C). No significant difference was observed for the MES responses (Figure 4C). We further calculated the surface DAT fraction using the Henderson-Hasselbalch equation and found that axonal shafts and boutons exhibited a similar ~75% surface fraction of DAT and similar acidity for DAT containing vesicles (Figures 4D and 4E). No significant difference was observed between TH+ and TH- neurons (Figure S4B). Varicosities, however, exhibited only ~20% surface DAT (Figure 4D) and DAT-containing

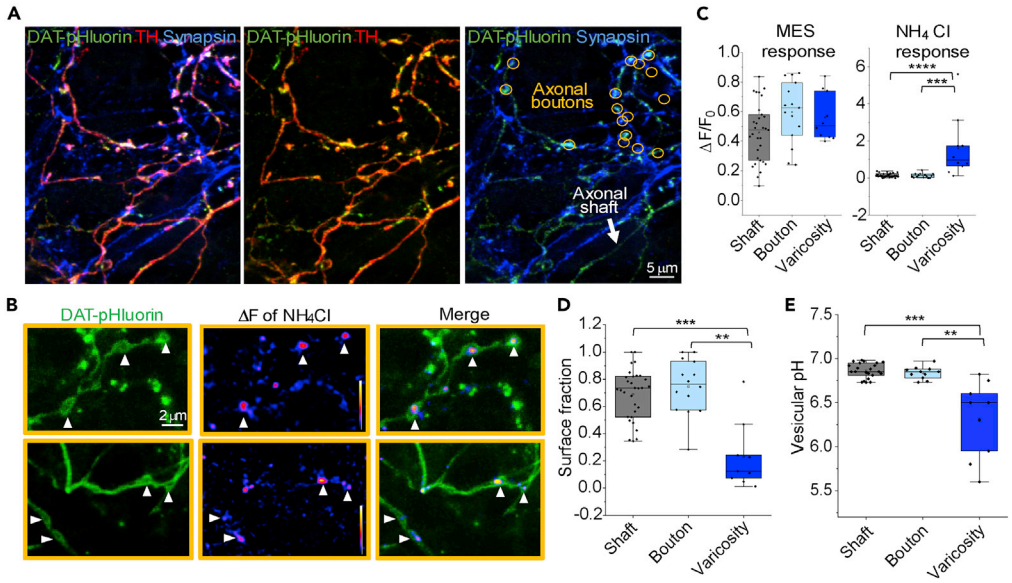

Figure 4. Varicosities contain a large portion of acidic intracellular DAT

(A) Representative immunofluorescence images of the axons expressing DAT-pH labeled with anti-GFP, anti-TH and anti-synapsin1/2. Orange circles indicate synapsin-enriched axonal boutons and the white arrow points to an axonal shaft with light synapsin staining.

(B) Representative axonal segments expressing DAT-pH and responded robustly to NH_4Cl perfusion. From left to right: DAT-pH axon at rest (left), the ΔF image of the NH_4Cl response of the axon (middle) and the overlay of the two images (right). The arrowheads point to varicosities with DAT-pH contours and NH_4Cl-responding centers.

(C) Box and whisker charts summarizing the MES and NH_4Cl responses for axonal shaft (N = 31), synapsin boutons (N = 15) and large varicosities (N = 10). F = 2.90, p = 0.064, one-way ANOVA for MES responses. Chi-Square = 19.62, ****p = 5.50E-5, Kruskal-Wallace test for NH_4Cl responses. ****p = 7.3E-5 comparing varicosity versus shaft, ***p = 8.41E-4 comparing varicosity versus bouton, p = 1.00 comparing bouton versus shaft, Mann-Whitney test with Bonferroni correction.

(D and E) Calculated surface fraction (D) and DAT-containing vesicular pH (E) based on the Henderson-Hasselbalch equation using the measurements in C. Data from four batches of cultures. Chi-Square = 16.45, ***p = 2.69E-4 Kruskal-Wallace test for surface fraction. ***p = 5.85E-4 comparing varicosity versus shaft, **p = 0.0018 comparing varicosity versus bouton, p = 0.96 comparing bouton versus shaft, Mann-Whitney test with Bonferroni correction. Chi-Square = 16.95, ***p = 2.09E-4 Kruskal-Wallace test for NH_4Cl responses. ***p = 3.45E-4 comparing varicosity versus shaft, **p = 0.0032 comparing varicosity versus bouton, p = 1.00 comparing bouton versus shaft, Mann-Whitney test with Bonferroni correction. See also Figure S4.

vesicles were substantially more acidic with an average pH of 6.31 ± 0.14 (Figure 4E). Thus, our data suggests that the constitutive recycling of DAT is similar between axonal shafts and synaptic boutons, whereas large varicosities stand out as unique structures potentially involved in DAT endocytosis and degradative processing.

Cocaine exposure elicits a redistribution of DAT to the axonal plasma membrane

Cocaine has been shown to not only inhibit DAT's reuptake activity but also to increase DAT surface expression,[15–17,19] or to prevent DAT from internalization.[18–20] The precise manner by which cocaine changes DAT surface expression/availability, especially in neurons, is not clear. An increase in DAT binding sites were reported in the striatal/synaptic regions of primates after chronic cocaine use.[59,60] In rodent models of substance use disorder, voltammetry studies have suggested reduced DA uptake, hence, less surface DAT in the nucleus accumbens (NAc) of mice given extended cocaine access,[61,62] whereas in the intermittent access model, an enhanced cocaine potency suggested increased DAT surface expression.[63]

To better understand cocaine-induced DAT trafficking in neurons, and to specifically pinpoint the changes of DAT surface expression in various subcellular compartments of the neuron, we expressed DAT-pH in cultured midbrain neurons and subjected the cell culture to either a 1-day or a 4-day cocaine (10 µM) treatment. We then compared surface DAT fraction and DAT-containing vesicular pH from cocaine treated cells

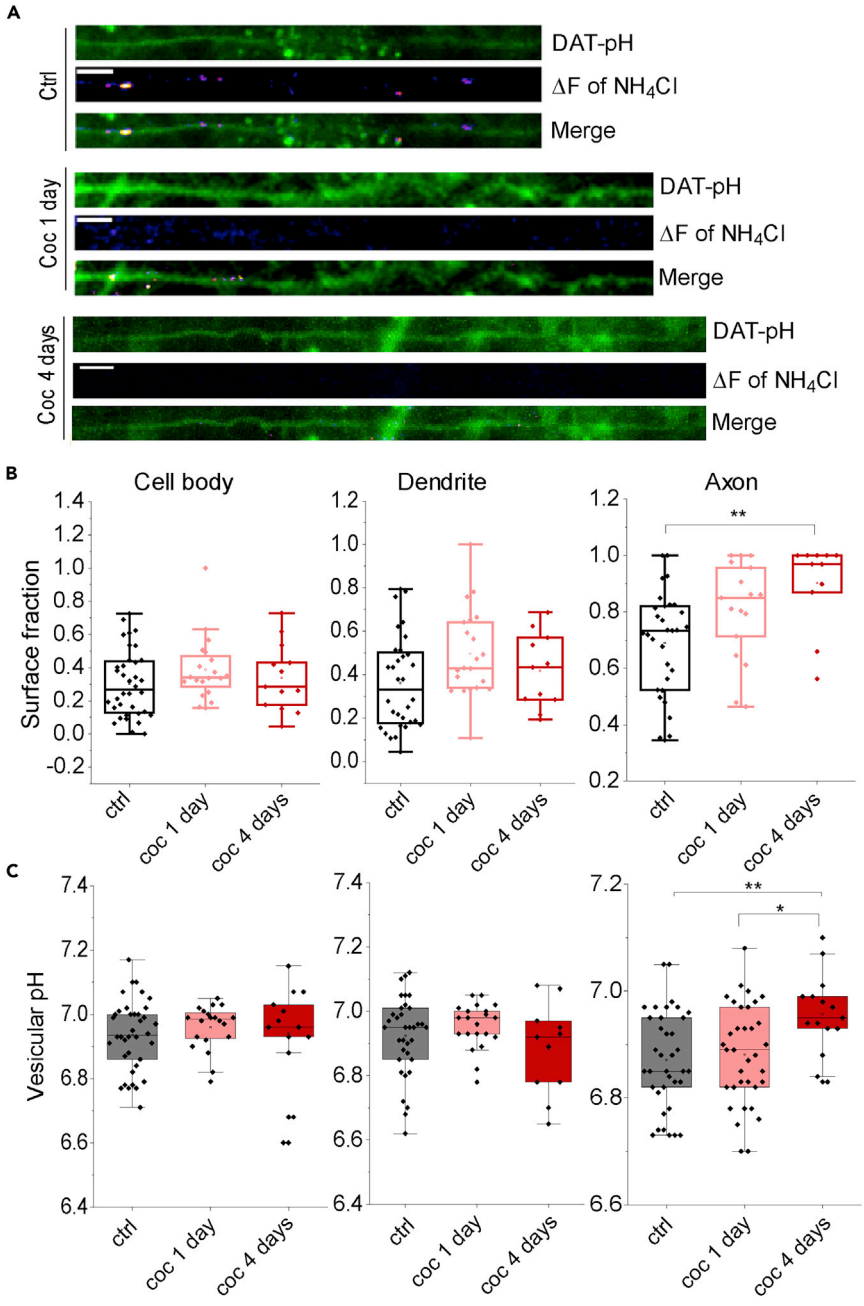

Figure 5. Cocaine exposure results in an increase in surface DAT fraction in the axon

(A) Representative NH4Cl responses (ΔF of NH4Cl) at the axon in cells without exposure to cocaine (control/ctrl), those that have been exposed to cocaine for 24 h (coc 1 day) and those that have been exposed to cocaine for 4 days (coc 4 days). The baseline DAT-pH images were shown above the NH4Cl ΔF images and the overlay images (merge) were shown at the bottom. Scale: 5 μm.

(B and C) Box and whisker plots for surface fraction (B) and vesicular pH (C) at the cell body, dendrites and axons in cocaine treated and non-treated neurons. Cell body: ctrl N = 32, coc 1 day N = 20, coc 4 days N = 13, F = 1.17, p = 0.32 for surface fraction and F = 0.34, p = 0.71 for vesicular pH, one-way ANOVA. Dendrite: ctrl N = 32, coc 1 day N = 21, coc 4 days N = 11, F = 2.78, p = 0.070 for surface fraction and F = 1.50, p = 0.23 for vesicular pH, one-way ANOVA. Axon: ctrl N = 31, coc 1 day N = 17, coc 4 days N = 11, Chi-Square = 12.57, **p = 0.0019 for surface fraction, Kruskal-Wallis ANOVA. **p = 0.0044 comparing ctrl versus coc 4 days, p = 0.098 comparing ctrl versus coc 1 day, p = 0.22 comparing coc 1day versus coc 4 days, Mann-Whitney test with Bonferroni correction. F = 5.19, p = 0.0075 for vesicular pH, one-day ANOVA. **p = 0.0071

Figure 5. *Continued*
comparing ctrl versus coc 4 days, *p = 0.023 comparing ctrl versus coc 1 day, p = 1.00 comparing coc 1day versus coc 4 days, Bonferroni post hoc following one-way ANOVA. Data from six batches of cultures for control, four batches of cultures for coc 1 day and three batches of cultures for coc 4 days.

to cells without cocaine treatment from the same batch. Of interest, DAT surface fraction remained relatively steady at the cell bodies and dendrites (Figure 5B). The axons exhibited a significant increase in surface DAT by day 4 (Figure 5B), which is consistent with the gradual reduction of the NH_4Cl response (Figure 5A) and a significant alkalization of the DAT-containing vesicles (Figure 5C).

The cocaine-induced DAT trafficking is regulated by synaptojanin1

To further investigate the mechanisms underlying cocaine-regulated DAT trafficking, we examined DAT-pH signals in response to a shorter cocaine treatment. Similar to the N2a cells (Figure 2F), neuronal cell bodies and axons exhibited a cocaine-induced reduction of DAT-pH fluorescence, which recovered and reversed to an increase in DAT-pH fluorescence within 5 min following cocaine removal (Figures 6A and 6B). Recent studies have suggested molecules important for clathrin coat removal, such as synaptojanin1 (Synj1) or auxilin1, play a crucial role in DAT expression and/or trafficking.[40,57,58] We therefore decided to investigate if Synj1 deficiency influences cocaine-regulated DAT trafficking using this new reporter. Of interest, in neurons carrying a heterozygous mutation of *Synj1* (*Synj1*$^{+/-}$), a larger deflection was observed (Figures 6A and 6B), which could suggest increased endocytosis of DAT or delivery of DAT to more acidic intracellular structures. Nonetheless, the slightly altered internalization phase did not impact the steady-state surface delivery of DAT-pH at the cell body (Figure 6A) but completely abolished this process in the axons of *Synj1*$^{+/-}$ neurons (Figure 6B). *Synj1* encodes a phosphoinositide phosphatase, synaptojanin1 (synj1) which has been well-characterized for its role in clathrin-mediated synaptic vesicle (SV) recycling.[37,38,40,41,64–66] Synj1 deletion results in an accumulation of clathrin-coated vesicles within the synaptic terminal.[36,37,67] Our data demonstrates the first evidence that Synj1 also regulates cocaine-induced DAT trafficking in the axons.

We next sought to determine the domain function of Synj1 involved in this regulation by expressing mutant human SYNJ1 (hSJ1) in N2a cells. In our previous work, we have shown that the Parkinson disease (PD)-linked R258Q mutation in the SAC1 phosphatase domain abolishes the PI(3)P and PI(4)P hydrolysis activities of the enzyme without affecting the primary 5′-phosphatase (5′-PPase) activity; however, the PD-linked R839C mutation reduces the $PI(4,5)P_2$ hydrolysis (by 60%) and abolishes PI(4)P hydrolysis (Figure 6C).[41] Mice carrying the Synj1 R258Q mutation exhibit DAT clusters specifically in the dorsal striatum,[40] suggesting dysregulation of DAT trafficking via the SAC1 enzyme. Another mutation in the 5′-PPase domain, hD769A/mD730A, which was previously reported to abolish the $PI(4,5)P_2$ hydrolysis[38] was also included in this analysis to perform a comprehensive dissection of the lipid signaling pathways. We found that wild-type (WT) SJ1 expression did not influence the surface delivery of DAT despite a smaller internalization response (Figure 6D). Both the RC and DA mutations interfered with DAT surface delivery, however, the RQ mutation in the SAC1 domain exhibited the most statistically significant impairment compared to the WT SJ1 (Figures 6D and 6E). Thus, our work using a newly engineered DAT optical reporter suggested an essential role of Synj1's phosphatase activities in cocaine-regulated DAT trafficking. Specifically, although the 5′-PPase is more important for gating DAT internalization, the SAC1 enzyme is perhaps essential, especially for neuronal axons, to support DAT surface delivery following internalization.

DISCUSSION

DAT trafficking is an integral part of DAT function and bears tremendous importance in DA-related disorders. However, our understanding on neuronal DAT trafficking is limited primarily because of the lack of research tools that are capable of revealing DAT trafficking events in small structures such as the axons. Here, we report the engineering of a DAT reporter, DAT-pH. We show that DAT-pH senses pH with a stable pKa of 7.0, while exhibiting DA uptake, cocaine sensitivity and regulated trafficking. We show that in cultured MB neurons, DAT-pH exhibit 25% of surface expression at cell bodies but 75% in axons. We further identified large varicosities as potential hotspots for axonal DAT internalization and degradation. Finally, we report a novel role of Synj1 in assisting cocaine-induced DAT trafficking to the axonal surface.

Compared to existing tools that measure DAT trafficking, DAT-pH offers multiple advantages: (1) DAT-pH is capable of revealing DAT localization or constitutive recycling in small neuronal structures that otherwise

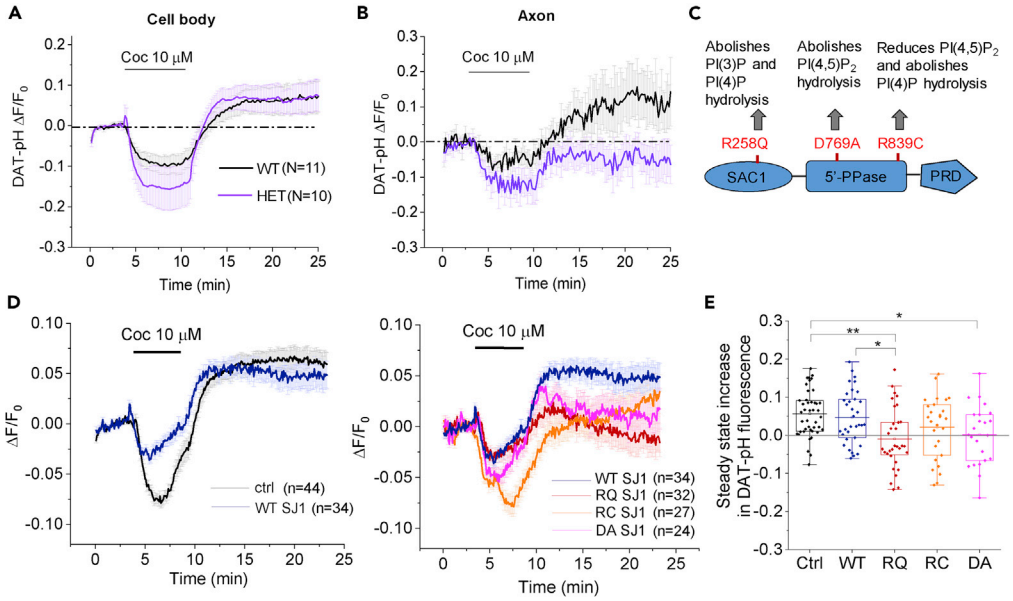

Figure 6. The cocaine-induced DAT trafficking is regulated by Synj1

(A and B) Averaged DAT-pH signals in response to an acute perfusion of cocaine measured from the cell body (A) or axon shafts (B) of the littermate MB neurons. Data is represented as mean ± SEM N = cell number from three independent batches of cultures.

(C) Synj1 domain structure, mutants used in the study and the previously reported impact of these mutations on phosphoinositide metabolism.

(D) Averaged DAT-pH signals in response to an acute perfusion of cocaine measured from control (ctrl) N2a cells or those transfected with WT hSJ1 or hSJ1 mutants. Left, overlay of the responses from control cells (black) and cells expressing WT SJ1 (navy). Right, overlay of the responses from WT and mutant SJ1 transfected cells. Data is represented as mean ± SEM from two independent batches of cultures. N = cell number.

(E) Box-whisker charts for the average of the final 3 min of the DAT-pH responses, which was denoted as steady state increase across all test groups. F = 5.21, p = 5.78E-4, one-way ANOVA. **p = 0.0014 comparing ctrl versus RQ, *p = 0.018 comparing WT versus RQ, *p = 0.041 comparing ctrl versus DA, p = 1.00 comparing WT vs. RC, p = 0.22 comparing WT versus DA, Bonferroni post hoc analysis following one-way ANOVA.

requires electron microscopy (EM) or super resolution imaging analysis. We report a compartmentalized expression pattern of DAT in neurons, which resembles previous EM analyses in rodent brains.[21,68,69] These results lend credibility to visualizing actual DAT trafficking events in neurons. (2) DAT-pH is a superior tool for revealing the dynamic changes of DAT in real-time for cell lines and neurons. Fluorescent DAT ligands, which have also been reported to label and track plasma membrane DAT,[7,8] often exhibit competitive binding with cocaine and native DA. Using DAT-pH we report for the first time the dynamic internalization and surface delivery of DAT on cocaine exposure, which is regulated by a phosphoinositol phosphatase, Synj1. It is also worth noting that although N2a cells initiated the reverse trafficking of DAT within 5 min of cocaine exposure, neurons did so after cocaine removal. These kinetic differences between a neuron and a heterologous cell, although not yet understood, would not be possible with conventional tools. (3) DAT-pH, being a genetically encoded reporter, has the potential to be used *in vivo* or in combination with another optical sensors, such as RdLight1[70] that measures DA. The DAT is an essential molecule for shaping DA transients in the brain, however, little is known about how trafficking of DAT is regulated by DA or other psychostimulants; and whether/how the translocation of DAT in turn modifies DA transients in the brain. For example, the somatodendritic DAT has been shown to not only mediate DA uptake but also participates in reverse transport of DA.[71–74] Thus, real-time measurement of DAT surface expression and DA transients may advance our understanding of DA signaling in an unprecedented way.

The DAT-pH reporter and its future derivatives are timely tools for investigators across the fields to understand DAT dysregulation in substance use disorders, affective disorders, and Parkinsonian neurodegeneration. Using DAT-pH we revealed a previously uncharacterized mode of axonal DAT trafficking especially in response to cocaine exposure. Interestingly, WT SJ1 overexpression resulted in a less robust internalization

but did not affect the steady state DAT surface expression. The RQ SJ1 induced a similar internalization as the WT SJ1 but failed to deliver DAT to the surface. Thus, the internalization phase that we observed appeared to be independent from DAT surface delivery. We are yet to understand the biological significance and the molecular mechanisms underlying the cocaine-induced DAT internalization. However, we are the first to demonstrate that the cocaine-induced surface expression of DAT is regulated by Synj1. Mutations in both phosphatases of *SYNJ1* have been implicated in early onset Parkinsonism.[75–78] Remarkably, genetic variants of *SYNJ1* are also associated with bipolar disorder.[79–81] The lack of ligand-induced DAT trafficking in the axons of *Synj1*$^{+/-}$ neurons may contribute to the altered DA signaling in the pathogenesis of these disorders, which we will investigated in the future. We envision that similar analyses can be carried out to assess other disease risk genes involved in PD, substance use disorders and psychosis.

Taken together, using a pH sensitive DAT reporter our study demonstrated previously uncharacterized biology of DAT trafficking in different parts of the neuron. We suggest immense potential for this reporter in revealing greater molecular details of DAT trafficking and DA signaling in physiological states as well as in disease pathogenesis.

Limitation of the study

There are a few limitations to be noted while interpreting data obtained using DAT-pH: First, DAT-pH measures pH rather than direct surface expression, which brings richness to the data (such as the DAT-containing vesicular pH) but also caveats when interpreting a singular measurement in a time-lapse study. Second, the DAT-pH analysis used in this study was unable to distinguish surface internalization from membrane lateral diffusion, another important form of DAT trafficking in the axon.[7,82] Indeed, we showed that the cocaine-induced increase in surface DAT at the cell body (Figure 6A) was not measurable after 24 h (Figure 5B), suggesting potential lateral diffusion. Future endeavors in developing ratiometric reporters for DAT would circumvent such concerns. Third, to apply DAT-pH analysis on small molecules known to induce DAT oligomerization,[20,83] we have yet to test in a more rigorous way whether DAT oligomerization would alter the pKa of DAT-pH. Lastly, the expression of the current DAT-pH in neuronal axons is relatively weak, which limits signal/noise ratio for axonal DAT trafficking and *in vivo* imaging at the striatum or nucleus accumbens. Further optimization of the reporter design is desired to expand the types of applications for DAT-pH.

STAR★METHODS

Detailed methods are provided in the online version of this paper and include the following:

- KEY RESOURCES TABLE
- RESOURCE AVAILABILITY
  - Lead contact
  - Materials availability
  - Data and code availability
- EXPERIMENTAL MODEL AND SUBJECT DETAILS
  - Animals
  - Cell lines
  - Primary cell culture
- METHOD DETAILS
  - Constructs and cloning
  - Cell culture transfection
  - Radioactive DA uptake assay
  - Live imaging and data processing
  - DAT-pH pKa measurements
  - Calculation for surface fraction and vesicular pH
  - JHC1-64 dye staining
  - Immunofluorescence and data analysis
  - Controlled substances
- QUANTIFICATION AND STATISTICAL ANALYSIS

SUPPLEMENTAL INFORMATION

Supplemental information can be found online at https://doi.org/10.1016/j.isci.2022.105782.

ACKNOWLEDGMENTS

We would like to thank Dr. Amy Newman for providing the cocaine analogue, JHC1-64 dye; Drs. Zhiping Pang, Timothy Ryan, and Jeffrey Diamond for providing valuable insight for the manuscript; and Dr. Loren Runnels for sharing the scintillation counter. The work is supported by an NINDS R01 grant (NS112390) awarded to P-Y.P., a Rutgers Brain Health Institute Pilot grant awarded to P-Y.P. and D.J.B., and a NINDS diversity supplement for J.S. (3R01NS112390-02S1).

AUTHOR CONTRIBUTIONS

J.S., D.J.B., and P-Y.P. conceptualized the project, J.S., O.Y., E.K., M.A., and P-Y.P. contributed to data collection and analysis. X.Z. and E.D-B. participated in the radioactive DA uptake study. D.J.B. and P-Y.P. obtained the funding. J.S. and P-Y.P. wrote the manuscript.

DECLARATION OF INTERESTS

The authors declare no competing interests.

INCLUSION AND DIVERSITY

One or more of the authors of this paper self-identifies as an underrepresented ethnic minority in their field of research or within their geographical location. One or more of the authors of this paper received support from a program designed to increase minority representation in their field of research.

Received: August 18, 2022
Revised: November 7, 2022
Accepted: December 7, 2022
Published: January 20, 2023

REFERENCES

1. Jones, S.R., Gainetdinov, R.R., Jaber, M., Giros, B., Wightman, R.M., and Caron, M.G. (1998). Profound neuronal plasticity in response to inactivation of the dopamine transporter. Proc. Natl. Acad. Sci. USA *95*, 4029–4034. https://doi.org/10.1073/pas.95.7.4029.

2. Zahniser, N.R., and Doolen, S. (2001). Chronic and acute regulation of Na+/Cl- -dependent neurotransmitter transporters: drugs, substrates, presynaptic receptors, and signaling systems. Pharmacol. Ther. *92*, 21–55. https://doi.org/10.1016/s0163-7258(01)00158-9.

3. Kahlig, K.M., and Galli, A. (2003). Regulation of dopamine transporter function and plasma membrane expression by dopamine, amphetamine, and cocaine. Eur. J. Pharmacol. *479*, 153–158. https://doi.org/10.1016/j.ejphar.2003.08.065.

4. Zahniser, N.R., and Sorkin, A. (2009). Trafficking of dopamine transporters in psychostimulant actions. Semin. Cell Dev. Biol. *20*, 411–417. https://doi.org/10.1016/j.semcdb.2009.01.004.

5. Zhu, J., and Reith, M.E.A. (2008). Role of the dopamine transporter in the action of psychostimulants, nicotine, and other drugs of abuse. CNS Neurol. Disord.: Drug Targets *7*, 393–409. https://doi.org/10.2174/187152708786927877.

6. Siciliano, C.A., Calipari, E.S., Ferris, M.J., and Jones, S.R. (2015). Adaptations of presynaptic dopamine terminals induced by psychostimulant self-administration. ACS Chem. Neurosci. *6*, 27–36. https://doi.org/10.1021/cn5002705.

7. Eriksen, J., Rasmussen, S.G.F., Rasmussen, T.N., Vaegter, C.B., Cha, J.H., Zou, M.F., Newman, A.H., and Gether, U. (2009). Visualization of dopamine transporter trafficking in live neurons by use of fluorescent cocaine analogs. J. Neurosci. *29*, 6794–6808. https://doi.org/10.1523/JNEUROSCI.4177-08.2009.

8. Guthrie, D.A., Klein Herenbrink, C., Lycas, M.D., Ku, T., Bonifazi, A., DeVree, B.T., Mathiasen, S., Javitch, J.A., Grimm, J.B., Lavis, L., et al. (2020). Novel fluorescent ligands enable single-molecule localization microscopy of the dopamine transporter. ACS Chem. Neurosci. *11*, 3288–3300. https://doi.org/10.1021/acschemneuro.0c00397.

9. Loder, M.K., and Melikian, H.E. (2003). The dopamine transporter constitutively internalizes and recycles in a protein kinase C-regulated manner in stably transfected PC12 cell lines. J. Biol. Chem. *278*, 22168–22174. https://doi.org/10.1074/jbc.M301845200.

10. Sorkina, T., Hoover, B.R., Zahniser, N.R., and Sorkin, A. (2005). Constitutive and protein kinase C-induced internalization of the dopamine transporter is mediated by a clathrin-dependent mechanism. Traffic *6*, 157–170. https://doi.org/10.1111/j.1600-0854.2005.00259.x.

11. Wheeler, D.S., Underhill, S.M., Stolz, D.B., Murdoch, G.H., Thiels, E., Romero, G., and Amara, S.G. (2015). Amphetamine activates Rho GTPase signaling to mediate dopamine transporter internalization and acute behavioral effects of amphetamine. Proc. Natl. Acad. Sci. USA *112*, E7138–E7147. https://doi.org/10.1073/pnas.1511670112.

12. Boudanova, E., Navaroli, D.M., and Melikian, H.E. (2008). Amphetamine-induced decreases in dopamine transporter surface expression are protein kinase C-independent. Neuropharmacology *54*, 605–612. https://doi.org/10.1016/j.neuropharm.2007.11.007.

13. Underhill, S.M., Hullihen, P.D., Chen, J., Fenollar-Ferrer, C., Rizzo, M.A., Ingram, S.L., and Amara, S.G. (2021). Amphetamines signal through intracellular TAAR1 receptors coupled to Galpha13 and GalphaS in discrete subcellular domains. Mol. Psychiatr. *26*, 1208–1223. https://doi.org/10.1038/s41380-019-0469-2.

14. Johnson, L.A., Furman, C.A., Zhang, M., Guptaroy, B., and Gnegy, M.E. (2005). Rapid delivery of the dopamine transporter to the plasmalemmal membrane upon amphetamine stimulation. Neuropharmacology *49*, 750–758. https://doi.org/10.1016/j.neuropharm.2005.08.018.

15. Saunders, C., Ferrer, J.V., Shi, L., Chen, J., Merrill, G., Lamb, M.E., Leeb-Lundberg, L.M., Carvelli, L., Javitch, J.A., and Galli, A. (2000). Amphetamine-induced loss of human dopamine transporter activity: an internalization-dependent and cocaine-sensitive mechanism. Proc. Natl. Acad. Sci. USA *97*, 6850–6855. https://doi.org/10.1073/pnas.110035297.

16. Little, K.Y., Elmer, L.W., Zhong, H., Scheys, J.O., and Zhang, L. (2002). Cocaine induction of dopamine transporter trafficking to the plasma membrane. Mol. Pharmacol. *61*, 436–445. https://doi.org/10.1124/mol.61.2.436.

17. Daws, L.C., Callaghan, P.D., Morón, J.A., Kahlig, K.M., Shippenberg, T.S., Javitch, J.A., and Galli, A. (2002). Cocaine increases dopamine uptake and cell surface expression of dopamine transporters. Biochem. Biophys. Res. Commun. *290*, 1545–1550. https://doi.org/10.1006/bbrc.2002.6384.

18. Underhill, S.M., Wheeler, D.S., Li, M., Watts, S.D., Ingram, S.L., and Amara, S.G. (2014). Amphetamine modulates excitatory neurotransmission through endocytosis of the glutamate transporter EAAT3 in dopamine neurons. Neuron *83*, 404–416. https://doi.org/10.1016/j.neuron.2014.05.043.

19. Siciliano, C.A., Saha, K., Calipari, E.S., Fordahl, S.C., Chen, R., Khoshbouei, H., and Jones, S.R. (2018). Amphetamine reverses escalated cocaine intake via restoration of dopamine transporter conformation. J. Neurosci. *38*, 484–497. https://doi.org/10.1523/JNEUROSCI.2604-17.2017.

20. Sorkina, T., Cheng, M.H., Bagalkot, T.R., Wallace, C., Watkins, S.C., Bahar, I., and Sorkin, A. (2021). Direct coupling of oligomerization and oligomerization-driven endocytosis of the dopamine transporter to its conformational mechanics and activity. J. Biol. Chem. *296*, 100430. https://doi.org/10.1016/j.jbc.2021.100430.

21. Block, E.R., Nuttle, J., Balcita-Pedicino, J.J., Caltagarone, J., Watkins, S.C., Sesack, S.R., and Sorkin, A. (2015). Brain region-specific trafficking of the dopamine transporter. J. Neurosci. *35*, 12845–12858. https://doi.org/10.1523/JNEUROSCI.1391-15.2015.

22. Miesenböck, G., De Angelis, D.A., and Rothman, J.E. (1998). Visualizing secretion and synaptic transmission with pH-sensitive green fluorescent proteins. Nature *394*, 192–195. https://doi.org/10.1038/28190.

23. Sankaranarayanan, S., De Angelis, D., Rothman, J.E., and Ryan, T.A. (2000). The use of pHluorins for optical measurements of presynaptic activity. Biophys. J. *79*, 2199–2208. https://doi.org/10.1016/S0006-3495(00)76468-X.

24. Pan, P.Y., Marrs, J., and Ryan, T.A. (2015). Vesicular glutamate transporter 1 orchestrates recruitment of other synaptic vesicle cargo proteins during synaptic vesicle recycling. J. Biol. Chem. *290*, 22593–22601. https://doi.org/10.1074/jbc.M115.651711.

25. Voglmaier, S.M., Kam, K., Yang, H., Fortin, D.L., Hua, Z., Nicoll, R.A., and Edwards, R.H. (2006). Distinct endocytic pathways control the rate and extent of synaptic vesicle protein recycling. Neuron *51*, 71–84. https://doi.org/10.1016/j.neuron.2006.05.027.

26. Pan, P.Y., Li, X., Wang, J., Powell, J., Wang, Q., Zhang, Y., Chen, Z., Wicinski, B., Hof, P., Ryan, T.A., and Yue, Z. (2017). Parkinson's disease-associated LRRK2 hyperactive kinase mutant disrupts synaptic vesicle trafficking in ventral midbrain neurons. J. Neurosci. *37*, 11366–11376. https://doi.org/10.1523/JNEUROSCI.0964-17.2017.

27. Pan, P.Y., and Ryan, T.A. (2012). Calbindin controls release probability in ventral tegmental area dopamine neurons. Nat. Neurosci. *15*, 813–815. https://doi.org/10.1038/nn.3099.

28. Araki, Y., Lin, D.T., and Huganir, R.L. (2010). Plasma membrane insertion of the AMPA receptor GluA2 subunit is regulated by NSF binding and Q/R editing of the ion pore. Proc. Natl. Acad. Sci. USA *107*, 11080–11085. https://doi.org/10.1073/pnas.1006584107.

29. Graves, A.R., Roth, R.H., Tan, H.L., Zhu, Q., Bygrave, A.M., Lopez-Ortega, E., Hong, I., Spiegel, A.C., Johnson, R.C., Vogelstein, J.T., et al. (2021). Visualizing synaptic plasticity in vivo by large-scale imaging of endogenous AMPA receptors. Elife *10*, e66809. https://doi.org/10.7554/eLife.66809.

30. Merrifield, C.J., Perrais, D., and Zenisek, D. (2005). Coupling between clathrin-coated-pit invagination, cortactin recruitment, and membrane scission observed in live cells. Cell *121*, 593–606. https://doi.org/10.1016/j.cell.2005.03.015.

31. Jullié, D., Stoeber, M., Sibarita, J.B., Zieger, H.L., Bartol, T.M., Arttamangkul, S., Sejnowski, T.J., Hosy, E., and von Zastrow, M. (2020). A discrete presynaptic vesicle cycle for neuromodulator receptors. Neuron *105*, 663–677.e8. https://doi.org/10.1016/j.neuron.2019.11.016.

32. Yu, Y.J., Dhavan, R., Chevalier, M.W., Yudowski, G.A., and von Zastrow, M. (2010). Rapid delivery of internalized signaling receptors to the somatodendritic surface by sequence-specific local insertion. J. Neurosci. *30*, 11703–11714. https://doi.org/10.1523/JNEUROSCI.6282-09.2010.

33. Ashrafi, G., Wu, Z., Farrell, R.J., and Ryan, T.A. (2017). GLUT4 mobilization supports energetic demands of active synapses. Neuron *93*, 606–615.e3. https://doi.org/10.1016/j.neuron.2016.12.020.

34. Burchfield, J.G., Lu, J., Fazakerley, D.J., Tan, S.X., Ng, Y., Mele, K., Buckley, M.J., Han, W., Hughes, W.E., and James, D.E. (2013). Novel systems for dynamically assessing insulin action in live cells reveals heterogeneity in the insulin response. Traffic *14*, 259–273. https://doi.org/10.1111/tra.12035.

35. McPherson, P.S., Garcia, E.P., Slepnev, V.I., David, C., Zhang, X., Grabs, D., Sossin, W.S., Bauerfeind, R., Nemoto, Y., and De Camilli, P. (1996). A presynaptic inositol-5-phosphatase. Nature *379*, 353–357. https://doi.org/10.1038/379353a0.

36. Cremona, O., Di Paolo, G., Wenk, M.R., Lüthi, A., Kim, W.T., Takei, K., Daniell, L., Nemoto, Y., Shears, S.B., Flavell, R.A., et al. (1999). Essential role of phosphoinositide metabolism in synaptic vesicle recycling. Cell *99*, 179–188. https://doi.org/10.1016/s0092-8674(00)81649-9.

37. Verstreken, P., Koh, T.W., Schulze, K.L., Zhai, R.G., Hiesinger, P.R., Zhou, Y., Mehta, S.Q., Cao, Y., Roos, J., and Bellen, H.J. (2003). Synaptojanin is recruited by endophilin to promote synaptic vesicle uncoating. Neuron *40*, 733–748. https://doi.org/10.1016/s0896-6273(03)00644-5.

38. Mani, M., Lee, S.Y., Lucast, L., Cremona, O., Di Paolo, G., De Camilli, P., and Ryan, T.A. (2007). The dual phosphatase activity of synaptojanin1 is required for both efficient synaptic vesicle endocytosis and reavailability at nerve terminals. Neuron *56*, 1004–1018. https://doi.org/10.1016/j.neuron.2007.10.032.

39. Dong, Y., Gou, Y., Li, Y., Liu, Y., and Bai, J. (2015). Synaptojanin cooperates in vivo with endophilin through an unexpected mechanism. Elife *4*, e05660. https://doi.org/10.7554/eLife.05660.

40. Cao, M., Wu, Y., Ashrafi, G., McCartney, A.J., Wheeler, H., Bushong, E.A., Boassa, D., Ellisman, M.H., Ryan, T.A., and De Camilli, P. (2017). Parkinson sac domain mutation in synaptojanin 1 impairs clathrin uncoating at synapses and triggers dystrophic changes in dopaminergic axons. Neuron *93*, 882–896.e5. https://doi.org/10.1016/j.neuron.2017.01.019.

41. Pan, P.Y., Sheehan, P., Wang, Q., Zhu, X., Zhang, Y., Choi, I., Li, X., Saenz, J., Zhu, J., Wang, J., et al. (2020). Synj1 haploinsufficiency causes dopamine neuron vulnerability and alpha-synuclein accumulation in mice. Hum. Mol. Genet. *29*, 2300–2312. https://doi.org/10.1093/hmg/ddaa080.

42. Vanhauwaert, R., Kuenen, S., Masius, R., Bademosi, A., Manetsberger, J., Schoovaerts, N., Bounti, L., Gontcharenko, S., Swerts, J., Vilain, S., et al. (2017). The SAC1 domain in synaptojanin is required for autophagosome maturation at presynaptic terminals. EMBO J. *36*, 1392–1411. https://doi.org/10.15252/embj.201695773.

43. Yang, S., Park, D., Manning, L., Hill, S.E., Cao, M., Xuan, Z., Gonzalez, I., Dong, Y., Clark, B., Shao, L., et al. (2022). Presynaptic autophagy is coupled to the synaptic vesicle cycle via ATG-9. Neuron *110*, 824–840.e10. https://doi.org/10.1016/j.neuron.2021.12.031.

44. Amara, S.G., and Kuhar, M.J. (1993). Neurotransmitter transporters: recent progress. Annu. Rev. Neurosci. *16*, 73–93. https://doi.org/10.1146/annurev.ne.16.030193.000445.

45. Beuming, T., Kniazeff, J., Bergmann, M.L., Shi, L., Gracia, L., Raniszewska, K., Newman, A.H., Javitch, J.A., Weinstein, H., Gether, U., and Loland, C.J. (2008). The binding sites for cocaine and dopamine in the dopamine transporter overlap. Nat. Neurosci. *11*, 780–789. https://doi.org/10.1038/nn.2146.

46. Li, L.B., Chen, N., Ramamoorthy, S., Chi, L., Cui, X.N., Wang, L.C., and Reith, M.E.A. (2004). The role of N-glycosylation in function and surface trafficking of the human dopamine transporter. J. Biol. Chem. *279*, 21012–21020. https://doi.org/10.1074/jbc.M311972200.

47. Nielsen, A.K., Möller, I.R., Wang, Y., Rasmussen, S.G.F., Lindorff-Larsen, K., Rand, K.D., and Loland, C.J. (2019). Substrate-induced conformational dynamics of the dopamine transporter. Nat. Commun. *10*, 2714. https://doi.org/10.1038/s41467-019-10449-w.

48. Sorkina, T., Richards, T.L., Rao, A., Zahniser, N.R., and Sorkin, A. (2009). Negative regulation of dopamine transporter endocytosis by membrane-proximal N-terminal residues. J. Neurosci. *29*, 1361–1374. https://doi.org/10.1523/JNEUROSCI.3250-08.2009.

49. Rao, A., Richards, T.L., Simmons, D., Zahniser, N.R., and Sorkin, A. (2012). Epitope-tagged dopamine transporter knock-in mice reveal rapid endocytic trafficking and filopodia targeting of the transporter in dopaminergic axons. Faseb. J. *26*, 1921–1933. https://doi.org/10.1096/fj.11-196113.

50. Sorkina, T., Miranda, M., Dionne, K.R., Hoover, B.R., Zahniser, N.R., and Sorkin, A. (2006). RNA interference screen reveals an essential role of Nedd4-2 in dopamine transporter ubiquitination and endocytosis. J. Neurosci. *26*, 8195–8205. https://doi.org/10.1523/JNEUROSCI.1301-06.2006.

51. Balaji, J., and Ryan, T.A. (2007). Single-vesicle imaging reveals that synaptic vesicle exocytosis and endocytosis are coupled by a single stochastic mode. Proc. Natl. Acad. Sci. USA *104*, 20576–20581. https://doi.org/10.1073/pnas.0707574105.

52. Cha, J.H., Zou, M.F., Adkins, E.M., Rasmussen, S.G.F., Loland, C.J., Schoenenberger, B., Gether, U., and Newman, A.H. (2005). Rhodamine-labeled 2beta-carbomethoxy-3beta-(3, 4-dichlorophenyl)tropane analogues as high-affinity fluorescent probes for the dopamine transporter. J. Med. Chem. *48*, 7513–7516. https://doi.org/10.1021/jm050431y.

53. Miranda, M., Wu, C.C., Sorkina, T., Korstjens, D.R., and Sorkin, A. (2005). Enhanced ubiquitylation and accelerated degradation of the dopamine transporter mediated by protein kinase C. J. Biol. Chem. *280*, 35617–35624. https://doi.org/10.1074/jbc.M506618200.

54. Carvelli, L., Morón, J.A., Kahlig, K.M., Ferrer, J.V., Sen, N., Lechleiter, J.D., Leeb-Lundberg, L.M.F., Merrill, G., Lafer, E.M., Ballou, L.M., et al. (2002). PI 3-kinase regulation of dopamine uptake. J. Neurochem. *81*, 859–869. https://doi.org/10.1046/j.1471-4159.2002.00892.x.

55. Matteoli, M., Coco, S., Schenk, U., and Verderio, C. (2004). Vesicle turnover in developing neurons: how to build a presynaptic terminal. Trends Cell Biol. *14*, 133–140. https://doi.org/10.1016/j.tcb.2004.01.007.

56. Gu, C. (2021). Rapid and reversible development of axonal varicosities: a new form of neural plasticity. Front. Mol. Neurosci. *14*, 610857. https://doi.org/10.3389/fnmol.2021.610857.

57. Ng, X.Y., Wu, Y., Lin, Y., Yaqoob, S.M., Greene, L.E., Camilli, P.D., and Cao, M. (2022). Synergistic Effect of Mutations in the Parkinson's Disease-Linked Endocytic Proteins Synaptojanin 1 (PARK20) and Auxilin (PARK19). Preprint at bioRxiv. https://doi.org/10.1101/2022.02.28.482419.

58. Vidyadhara, D.J., Somayaji, M., Wade, N., Yücel, B., Zhao, H., Shashaank, N., Ribaudo, J., Gupta, J., Lam, T.T., Sames, D., et al. (2022). Dopamine transporter and synaptic vesicle sorting defects initiate auxilin-linked Parkinson's disease. Preprint at bioRxiv. https://doi.org/10.1101/2022.02.04.479203.

59. Letchworth, S.R., Nader, M.A., Smith, H.R., Friedman, D.P., and Porrino, L.J. (2001). Progression of changes in dopamine transporter binding site density as a result of cocaine self-administration in rhesus monkeys. J. Neurosci. *21*, 2799–2807.

60. Mash, D.C., Pablo, J., Ouyang, Q., Hearn, W.L., and Izenwasser, S. (2002). Dopamine transport function is elevated in cocaine users. J. Neurochem. *81*, 292–300. https://doi.org/10.1046/j.1471-4159.2002.00820.x.

61. Calipari, E.S., Ferris, M.J., Melchior, J.R., Bermejo, K., Salahpour, A., Roberts, D.C.S., and Jones, S.R. (2014). Methylphenidate and cocaine self-administration produce distinct dopamine terminal alterations. Addiction Biol. *19*, 145–155. https://doi.org/10.1111/j.1369-1600.2012.00456.x.

62. Ferris, M.J., Calipari, E.S., Mateo, Y., Melchior, J.R., Roberts, D.C.S., and Jones, S.R. (2012). Cocaine self-administration produces pharmacodynamic tolerance: differential effects on the potency of dopamine transporter blockers, releasers, and methylphenidate. Neuropsychopharmacology *37*, 1708–1716. https://doi.org/10.1038/npp.2012.17.

63. Calipari, E.S., Ferris, M.J., Zimmer, B.A., Roberts, D.C.S., and Jones, S.R. (2013). Temporal pattern of cocaine intake determines tolerance vs sensitization of cocaine effects at the dopamine transporter. Neuropsychopharmacology *38*, 2385–2392. https://doi.org/10.1038/npp.2013.136.

64. de Heuvel, E., Bell, A.W., Ramjaun, A.R., Wong, K., Sossin, W.S., and McPherson, P.S. (1997). Identification of the major synaptojanin-binding proteins in brain. J. Biol. Chem. *272*, 8710–8716. https://doi.org/10.1074/jbc.272.13.8710.

65. Milosevic, I., Giovedi, S., Lou, X., Raimondi, A., Collesi, C., Shen, H., Paradise, S., O'Toole, E., Ferguson, S., Cremona, O., and De Camilli, P. (2011). Recruitment of endophilin to clathrin-coated pit necks is required for efficient vesicle uncoating after fission. Neuron *72*, 587–601. https://doi.org/10.1016/j.neuron.2011.08.029.

66. Watanabe, S., Mamer, L.E., Raychaudhuri, S., Luvsanjav, D., Eisen, J., Trimbuch, T., Söhl-Kielczynski, B., Fenske, P., Milosevic, I., Rosenmund, C., and Jorgensen, E.M. (2018). Synaptojanin and endophilin mediate neck formation during ultrafast endocytosis. Neuron *98*, 1184–1197.e6. https://doi.org/10.1016/j.neuron.2018.06.005.

67. Harris, T.W., Hartwieg, E., Horvitz, H.R., and Jorgensen, E.M. (2000). Mutations in synaptojanin disrupt synaptic vesicle recycling. J. Cell Biol. *150*, 589–600. https://doi.org/10.1083/jcb.150.3.589.

68. Hersch, S.M., Yi, H., Heilman, C.J., Edwards, R.H., and Levey, A.I. (1997). Subcellular localization and molecular topology of the dopamine transporter in the striatum and substantia nigra. J. Comp. Neurol. *388*, 211–227.

69. Nirenberg, M.J., Vaughan, R.A., Uhl, G.R., Kuhar, M.J., and Pickel, V.M. (1996). The dopamine transporter is localized to dendritic and axonal plasma membranes of nigrostriatal dopaminergic neurons. J. Neurosci. *16*, 436–447.

70. Patriarchi, T., Mohebi, A., Sun, J., Marley, A., Liang, R., Dong, C., Puhger, K., Mizuno, G.O., Davis, C.M., Wiltgen, B., et al. (2020). An expanded palette of dopamine sensors for multiplex imaging in vivo. Nat. Methods *17*, 1147–1155. https://doi.org/10.1038/s41592-020-0936-3.

71. Falkenburger, B.H., Barstow, K.L., and Mintz, I.M. (2001). Dendrodendritic inhibition through reversal of dopamine transport. Science *293*, 2465–2470. https://doi.org/10.1126/science.1060645.

72. Opazo, F., Schulz, J.B., and Falkenburger, B.H. (2010). PKC links Gq-coupled receptors to DAT-mediated dopamine release. J. Neurochem. *114*, 587–596. https://doi.org/10.1111/j.1471-4159.2010.06788.x.

73. Rice, M.E., and Patel, J.C. (2015). Somatodendritic dopamine release: recent mechanistic insights. Philos. Trans. R. Soc. Lond. B Biol. Sci. *370*, 20140185. https://doi.org/10.1098/rstb.2014.0185.

74. Sulzer, D., Cragg, S.J., and Rice, M.E. (2016). Striatal dopamine neurotransmission: regulation of release and uptake. Basal Ganglia *6*, 123–148. https://doi.org/10.1016/j.baga.2016.02.001.

75. Krebs, C.E., Karkheiran, S., Powell, J.C., Cao, M., Makarov, V., Darvish, H., Di Paolo, G., Walker, R.H., Shahidi, G.A., Buxbaum, J.D., et al. (2013). The Sac1 domain of SYNJ1 identified mutated in a family with early-onset progressive Parkinsonism with generalized seizures. Hum. Mutat. *34*, 1200–1207. https://doi.org/10.1002/humu.22372.

76. Quadri, M., Fang, M., Picillo, M., Olgiati, S., Breedveld, G.J., Graafland, J., Wu, B., Xu, F., Erro, R., Amboni, M., et al. (2013). Mutation in the SYNJ1 gene associated with autosomal recessive, early-onset Parkinsonism. Hum. Mutat. *34*, 1208–1215. https://doi.org/10.1002/humu.22373.

77. Kirola, L., Behari, M., Shishir, C., and Thelma, B.K. (2016). Identification of a novel homozygous mutation Arg459Pro in SYNJ1 gene of an Indian family with autosomal recessive juvenile Parkinsonism. Park. Relat. Disord. *31*, 124–128. https://doi.org/10.1016/j.parkreldis.2016.07.014.

78. Taghavi, S., Chaouni, R., Tafakhori, A., Azcona, L.J., Firouzabadi, S.G., Omrani, M.D.,

Jamshidi, J., Emamalizadeh, B., Shahidi, G.A., Ahmadi, M., et al. (2018). A clinical and molecular genetic study of 50 families with autosomal recessive parkinsonism revealed known and novel gene mutations. Mol. Neurobiol. *55*, 3477–3489. https://doi.org/10.1007/s12035-017-0535-1.

79. Horschitz, S., Hummerich, R., Lau, T., Rietschel, M., and Schloss, P. (2005). A dopamine transporter mutation associated with bipolar affective disorder causes inhibition of transporter cell surface expression. Mol. Psychiatr. *10*, 1104–1109. https://doi.org/10.1038/sj.mp.4001730.

80. Saito, T., Guan, F., Papolos, D.F., Lau, S., Klein, M., Fann, C.S., and Lachman, H.M. (2001). Mutation analysis of SYNJ1: a possible candidate gene for chromosome 21q22-linked bipolar disorder. Mol. Psychiatr. *6*, 387–395. https://doi.org/10.1038/sj.mp.4000871.

81. Kato, T., Kakiuchi, C., and Iwamoto, K. (2007). Comprehensive gene expression analysis in bipolar disorder. Can. J. Psychiatr. *52*, 763–771. https://doi.org/10.1177/070674370705201203.

82. Bagalkot, T.R., Block, E.R., Bucchin, K., Balcita-Pedicino, J.J., Calderon, M., Sesack, S.R., and Sorkin, A. (2021). Dopamine transporter localization in medial forebrain bundle axons indicates its long-range transport primarily by membrane diffusion with a limited contribution of vesicular traffic on retromer-positive compartments. J. Neurosci. *41*, 234–250. https://doi.org/10.1523/JNEUROSCI.0744-20.2020.

83. Sorkina, T., Ma, S., Larsen, M.B., Watkins, S.C., and Sorkin, A. (2018). Small molecule induced oligomerization, clustering and clathrin-independent endocytosis of the dopamine transporter. Elife *7*, e32293. https://doi.org/10.7554/eLife.32293.

84. Schneider, C.A., Rasband, W.S., and Eliceiri, K.W. (2012). NIH Image to ImageJ: 25 years of image analysis. Nat. Methods *9*, 671–675. https://doi.org/10.1038/nmeth.2089.

85. Miura, H., Matsuda, M., and Aoki, K. (2014). Development of a FRET biosensor with high specificity for Akt. Cell Struct. Funct. *39*, 9–20. https://doi.org/10.1247/csf.13018.

86. Aggarwal, S., and Mortensen, O.V. (2017). In vitro assays for the functional characterization of the dopamine transporter (DAT). Curr. Protoc. Pharmacol. *79*, 12.17.1–12.17.21. https://doi.org/10.1002/cpph.33.

87. Sun, W.L., Quizon, P.M., Yuan, Y., Zhang, W., Ananthan, S., Zhan, C.G., and Zhu, J. (2017). Allosteric modulatory effects of SRI-20041 and SRI-30827 on cocaine and HIV-1 Tat protein binding to human dopamine transporter. Sci. Rep. *7*, 3694. https://doi.org/10.1038/s41598-017-03771-0.

88. Mitchell, S.J., and Ryan, T.A. (2004). Syntaxin-1A is excluded from recycling synaptic vesicles at nerve terminals. J. Neurosci. *24*, 4884–4888. https://doi.org/10.1523/JNEUROSCI.0174-04.2004.

STAR★METHODS

KEY RESOURCES TABLE

REAGENT or RESOURCE	SOURCE	IDENTIFIER
Antibodies		
Chicken anti-GFP	Thermo Fisher	Cat# A-10262; RRID: AB_2534023
Rabbit anti-GFP	Thermo Fisher	Cat# A-11122; RRID: AB_221569
Guinea pig anti-synapsin1/2	Synaptic System	Cat#106004; RRID: AB_1106784
Mouse anti-TH	Sigma	Cat# T2928; RRID: AB_477569
Rabbit anti-TH	Novus Biologicals	Cat# NB300-109; RRID: AB_10077691
Rat anti-DAT	Millipore	Cat# MAB369; RRID: AB_2190413
Bacterial and virus strains		
Bacteria: DH5α	Thermo Fisher	Cat# 18265017
Bacteria: XL-10 Gold	Agilent Technology	Cat# 200314
Chemicals, peptides, and recombinant proteins		
Cytosine β-D-arabinofuranoside hydrochloride (ARA-C)	Sigma-Aldrich	Cat# C6645
Cocaine hydrochloride	Sigma-Aldrich	Cat# C5776
^{3}H-DA (Dihydroxyphenylethylamine (Dopamine), 3,4-[Ring-2,5,6-3H]-, 250 μCi (9.25MBq)	PerkinElmer	Cat# NET673250UC
D-Amphetamine Hemisulfate Salt	Sigma-Aldrich	Cat# A5880
Experimental models: Cell lines		
Neuro-2a (N2a) cells	ATCC	Cat# CCL-131; RRID: CVCL_0470
SH-SY5Y cells	ATCC	Cat# CRL-2266; RRID: CVCL_0019
Experimental models: Organisms/strains		
C57BL/6J mice	IMSR_JAX:	Cat# 000664; RRID: IMSR_JAX:000,664
Synj1+/- mice	Pietro DeCamilli laboratory at Yale University	N/A
Oligonucleotides		
DAT-N Forward: cgagctcaagcttcgaattctgcagtcgacgg	This paper	N/A
DAT-N_194 Reverse: gctagtgctaccggtaggatgggcatc	This paper	N/A
DAT-C_195 Forward: tagtggcaccggtggtgactccagtgg	This paper	N/A
DAT-C Reverse: cggacggtctagagccggtggatcccgg	This paper	N/A
CFP Forward: gctagcgctaccggtcaagaattcgccacc	This paper	N/A
CFP Reverse: aattcactcctcaggcgaattctgcagtcg	This paper	N/A
Recombinant DNA		
Plasmid: pEYFP-C1-DAT	Addgene	Cat# 90228; RRID: Addgene_90228

(*Continued on next page*)

Continued

REAGENT or RESOURCE	SOURCE	IDENTIFIER
Plasmid: tagRFP-C1-DAT-HA	Addgene	Cat# 90265; RRID: Addgene_90265
Plasmid: pCAG-ECFP	Addgene	Cat# 32597; RRID: Addgene_32597
Plasmid: vGlut1-pHluorin	Timothy A. Ryan laboratory at Weill Cornell Medical College	N/A
Plasmid: Eevee-iAkt-PM	Kazuhiro Aoki at National Institute for Basic Biology, Japan	N/A
Software and algorithms		
ImageJ	Schneider et al.[84]	https://imagej.nih.gov/ij/
OriginPro 2018/2023	Origin Lab	https://www.originlab.com/
Other		
JHC1-64 dye	Amy Newman Laboratory at NIH	N/A

RESOURCE AVAILABILITY

Lead contact

Further information and requests for resources and reagents should be directed to and will be fulfilled by the lead contact, Ping-Yue Pan (pingyue.pan@rutgers.edu).

Materials availability

DAT-pHluorin generated in this study will be shared by the lead contact upon request.

Data and code availability

- All data reported in this paper will be shared by the lead contact upon request.
- This paper does not report original code.
- Any additional information required to reanalyze the data reported in this paper is available from the lead contact upon request.

EXPERIMENTAL MODEL AND SUBJECT DETAILS

Animals

C57BL/6J mice (RRID: IMSR_JAX:000664) were originally purchased from the Jax lab. The *Synj1+/-* mice[36] were gifted by the Pietro DeCamilli laboratory at Yale University. *Synj1+/-* mice were crossed to the C57BL/6J mice to generate littermate pups for MB cultures. Mice were housed in the pathogen-free barrier facility at the Rutgers Robert Wood Johnson Medical School SPH vivarium. Handling procedures were in accordance with the National Institutes of Health guidelines approved by the Institutional Animal Care and Use Committee (IACUC # PROTO201800183). Both male and female mice were used for preparing primary neuron cultures.

Cell lines

N2a cells (RRID: CVCL_0470) from male origin were cultured and passaged following an ATCC suggested protocol using culture media containing DMEM (Thermo Fisher, 11965118), 10% fetal bovine serum (FBS) (Atlantic Biologicals, S11550), and 5% 10 U/mL Penicillin-Streptomycin (Thermo Fisher, 15140122). Cells were trypsinized using 0.05% Trypsin-EDTA (Gibco, 25300-054) and plated at 30% confluency.

SH-SY5Y cells (RRID: CVCL_0019) of female origin were cultured and passaged according to the ATCC suggested protocol using DMEM/F-12(1:1) culture media (Gibco, 11320-033) containing 10% FBS (Atlantic Biologicals, S11550), and 5%10 U/mL Penicillin-Streptomycin (Thermo Fisher, 15140122). For experiments, cells were trypsinized using 0.05% Trypsin-EDTA and plated at 50% confluency.

Primary cell culture

Midbrain cultures[26,27] were prepared as described previously. Ventral midbrains (containing both VTA and SN) were dissected from P0 male and female mouse pups and digested using papain (Worthington, LK003178) in a 35 °C water bath with gentle stirring and constant oxygenation. Midbrain neurons were then seeded within a cloning cylinder on the #1.5 cover glasses pretreated with Poly-L-ornithine (Sigma, P3655). Cells were plated at a density of 199,000 cells/cm^2 and grown in the Neurobasal-A based medium supplemented with GDNF (10 ng/mL, EMD Millipore, GF030).

METHOD DETAILS

Constructs and cloning

Human DAT cDNA was amplified from YFP-hDAT (Addgene, 90228) and pHluorin was amplified from vGlut1-pHluorin (a gift from Timothy A. Ryan and pHluorin is an original asset of James E. Rothman). The hDAT-pHluorin cDNA was inserted in the modified pCAGGS backbone (cut out from the Eevee-iAkt-pm sensor,[85] a gift from Kazuhiro Aoki) using the ECoR-I and Xba-I restriction sites. The plasmid contains a CAG (combination of chicken beta-actin promoter with CMV enhancer) promotor. An Age-I restriction site was inserted first by two-step PCR amplification using primers at the desired position of hDAT, followed by enzyme digestion and pHluorin insertion. The same linkers in vGlut1-pHluorin were used (TGSTSGGSGGTGG and SGGTGGSGGTGGSGGTG) on both ends of pHluorin in DAT-pH. The correct orientation of the pHluorin was confirmed by sequencing. DAT-HA was amplified from RFP-HA-DAT (Addgene, 90265) using ECoR-I and Xba-I sites and subcloned into the same backbone as the DAT-pH. All primers were synthesized by IDT custom DNA oligo services and all subcloning enzymes and buffers were purchased from New England Biolabs (NEB). DH5α (Thermo Fisher, 18265017) or XL-10 Gold (Agilent Technology, 200314) competent cells were used for plasmid amplification.

The following constructs were purchased directly from Addgene: pEYFP-C1-DAT (90228), tagRFP-C1-DAT-HA (90265) and pCAG-ECFP (32597). CFP-DAT was subcloned using the following primers: forward-5′-gctagcgctaccggtcaagaattcgccacc-3′ and reverse-5′-aattcactcctcaggcgaattctgcagtcg-3′ to replace EYFP using the Age-I and EcoR-I enzymatic sites.

Cell culture transfection

For N2a cells and SH-SY5Y cells, transfection was carried out following a company suggested protocol the day after plating using Lipofectamine^{TM}3000 (Thermo Fisher, L3000015). The transfection mixture was left in the medium until the day of imaging (typically within 24-48). For primary neurons, Lipofectamine^{TM} 2000 (Thermo Fisher, 11668019) was used for transfection at DIV (days *in vitro*) 7 following a company suggested protocol. The DNA-lipofectamine mixture was washed out after 45 min incubation at 37 °C and the growth medium was replaced with a fresh medium supplemented with an antimitotic agent, ARA-C (Sigma-Aldrich, C6645).

Radioactive DA uptake assay

Radioactive DA uptake assay was performed following previous published protocols.[86] N2a cells and SH-SY5Y cells were seeded in triplicates in the 24-well plate two days before the uptake assay. Cells typically reach 80% confluency on day of testing. For cocaine inhibition, cells were treated with 10 μM cocaine (Sigma, C5776) for 50 min in the cell culture incubator prior to the uptake assay based on published results to achieve maximum inhibition.[87] ^{3}H-DA (Dihydroxyphenylethylamine (Dopamine), 3,4-[Ring-2,5,6-3H]-, 250μCi (9.25MBq)) was purchased from PerkinElmer (NET673250UC). 50 nM ^{3}H-DA was diluted in the uptake buffer containing 130 mM NaCl, 1.3 mM KCl, 10 mM HEPES, 1.2 mM $MgSO_4$, 1.2 mM KH_2PO4, 2.2 mM $CaCl_2$, 10 mM glucose as well as 50 mM L(+) ascorbic acid (Millipore, AX1775-3) and 50 mM pargyline (Sigma Aldrich, P8013.) from freshly prepared stock before the experiment. 10 μM cocaine was added when testing cocaine inhibition. The pH of the buffer was adjusted to 7.4. Cells were incubated with the ^{3}H-DA at room temperature for 10 min before washing with an additional uptake buffer without ^{3}H-DA. Scintillation fluid was added to the wells immediately and transferred to the tubes. The radioactive signal was read by the scintillation counter (Beckman, LS 6500). For cocaine inhibition analysis, duplicate cultures were made for Western blot analysis and all uptake counts were normalized to the total DAT proteins in the culture.

Live imaging and data processing

For live cell imaging, cells on cover glass were mounted on a custom-made laminar-flow chamber with constant gravity perfusion (at a rate of ~0.2-0.3 mL/min) of a Tyrode's salt solution containing 119 mM NaCl, 2.5 mM KCl, 2 mM $CaCl_2$, 2 mM $MgCl_2$, 25 mM HEPES, 30 mM Glucose, 10 μM 6-cyano-7-nitroquinoxaline-2,3-dione (CNQX), and 50 μM D, L-2-amino-5-phosphonovaleric acid (AP-5) and buffered to pH 7.40. The NH_4Cl medium contains: 50 mM NH_4Cl, 70 mM NaCl, 2.5 mM KCl, 2 mM $CaCl_2$, 2 mM $MgCl_2$, 25 mM HEPES, 30 mM Glucose, 10 μM CNQX, and 50 μM AP-5, buffered to pH 7.40. The MES medium contains: 25 mM MES, 70 mM NaCl, 2.5 mM KCl, 2 mM $CaCl_2$, 2 mM $MgCl_2$, 30 mM Glucose, 10 μM CNQX, and 50 μM AP-5, buffered to pH 5.50. Perfusion of Tyrode's solution is regulated by Valvelink 8.2 and the NH_4Cl or MES solutions were perfused by pipettes. All chemicals were purchased from Sigma-Aldrich. Temperature was clamped at ~31.0 °C on the objective throughout the experiment. Images were acquired using a highly sensitive, back-illuminated EM-CCD camera (iXon+ Model DU-897E-BV, Andor Corp., CT, USA). Nikon Ti-2 wide-field microscope is modified with Spectra-X (Lumencor) as the light source for shuttered illumination. pHluorin fluorescence excitation and collection were using a Nikon PLan APO 60X 1.40 NA objective using 525/50m emission filter and 495LP dichroic filters (Chroma, 49002).

Images were sampled at 1 Hz using the Elements software and analyzed in ImageJ. Cell body responses were measured by regions of interests (ROIs) drawn by the freehand tool based on the ΔF image of the NH_4Cl response. Dendritic responses were measured using the 8x8 pixels (2 μM) circular ROIs based on the ΔF image of the NH_4Cl response. Axonal responses were measured using the 6x6 pixels (1.5 μM) circular ROIs based on the basal fluorescence image and the ΔF image of the MES response. For varicosity of a large size, several circular ROIs might be placed to cover the area. The average response of all ROIs from one of the three above compartments (cell body, dendrite or axon) was extracted using the Time Series Analyzer plugin. All responses were background subtracted followed by baseline normalization in OriginLabs. Typically, two or three trials of sequential perfusions were carried out with 5-10 min spacing for each imaging field and the averaged peak response was measured as the MES or the NH_4Cl response of the cell.

DAT-pH pKa measurements

Measurements were made at midbrain neuron axons due to the highest surface fraction and least interference with endogenous buffers. For the pH 5.50 and pH 5.60 solutions we used 25 mM MES (pKa 6.1) (Millipore-Sigma, M3671) to replace HEPES in Tyrode's. For the pH 8.50 and pH 9.50 solutions we used 25 mM BICINE (pKa 8.3) (Millipore-Sigma, B3876) to replace HEPES in Tyrode's. All solutions were perfused by hand pipetting during a period of 5 min imaging. Typically, data from each axon is averaged from two sequential perfusion experiments. DAT-pH fluorescence changes were normalized to the peak ΔF.

Calculation for surface fraction and vesicular pH

The calculation of surface fraction and vesicular pH was performed following previous published methods.[88] At any given pH (pH_i), the deprotonated DAT-pHluorin molecules determines the fluorescence. Based on the Henderson-Hasselbalch equation, the fluorescence change during perfusion of a pH 7.4 membrane permeable NH_4Cl solution is determined by the following function assuming pKa = 7.0:

$$dx = \frac{\left(1/\left(1+10^{7.0-7.4}\right) - 1/\left(1+10^{7.0-\mathrm{pHi}}\right)\right)}{1/\left(1+10^{7.0-\mathrm{pH_i}}\right)}$$

The surface fraction as a function of pH_i is then plotted by

$$Fr = \frac{\mathrm{dx} - \frac{\mathrm{dF}}{\mathrm{F0}}\text{of NH4Cl response}}{\mathrm{dx} * \frac{\mathrm{dF}}{\mathrm{F0}}\text{of NH4Cl response} + \mathrm{dx}}$$

During perfusion of a pH 5.5 MES solution, the ratio of surface to internal DAT-pH can be calculated as the following

$$\Phi = \frac{1/\left(1+10^{7.0-5.5}\right)}{1/\left(1+10^{7.0-\mathrm{pHi}}\right)}$$

The surface fraction as a function of pH_i is then plotted by

$$Fr = \frac{\frac{dF}{F0}\text{ of MES response}}{1 - dx + \Phi * \left(1 - \frac{dF}{F0}\text{ of MES response}\right)}$$

The surface fraction and vesicular pH are determined at the point where two functions intersect.

JHC1-64 dye staining

Staining was performed following previously published protocols.[7,8] Briefly, midbrain cultures were washed three times in ice old JHC-buffer containing: 25 mM HEPES, pH 7.4, with 130 mM NaCl, 5.4 mM KCl, 1.2 mM $CaCl_2$, 1.2 mM $MgSO_4$, 1 mM L-ascorbic acid, 5 mM D-glucose. Cell culture was then incubated with 50 nM JHC1-64 dye diluted in JHC buffer at 4°C for 30 min. After incubation the dye was washed away three times with ice-cold JHC- buffer followed by immediate fixation with 4% PFA at room temperature.

Immunofluorescence and data analysis

Immunocytochemistry was performed following previously published procedures.[26,27] The following antibodies were used for immunofluorescence: chicken anti-GFP (Thermo Fisher, A-10262, 1:1000), rabbit ant-GFP (Thermo Fisher, A-11122, 1:1000). Guinea pig anti-synapsin 1/2 (Synaptic System, 106004, 1:500), mouse anti-TH (Sigma, T2928, 1:1000), rabbit anti-TH (Novus Biologicals, NB300-109, 1:1000), rat anti-DAT (Millipore MAB369 1:1000), Immunofluorescence was analyzed using a Nikon Ti-2 wide-field microscope or a Nikon CREST spinning disk confocal microscope. The same imaging parameters were set for each batch of culture. Image stacks were taken at different focal planes at 0.9 μm interval to include the whole cell and a maximum projection image was generated for each stack via ImageJ for analysis. All analyses were done manually. Synapsin 1/2-positive boutons were determined based on the bright punctate staining pattern.

Controlled substances

Cocaine hydrochloride (Sigma C5776) and D-Amphetamine Hemisulfate Salt (Sigma A5880) were purchased from Sigma through authorized institutional distributors. For cocaine experiments, cells were treated with 10 μM cocaine for 24 (1 day) or for 4 consecutive days. Treatment typically starts on DIV (days *in vitro*) 12-13 and imaging experiments were performed between DIV 13 and DIV 17.

QUANTIFICATION AND STATISTICAL ANALYSIS

All data are replicated within the same batch and across multiple batches of cells. For datasets that follow normal distribution and exhibit equal variance, Student's *t* test or ANOVA test was used, followed by Bonferroni correction for *post hoc* analysis. For datasets that reject normal distribution and exhibit non-homogenous variance, Mann-Whitney test or Kruskal Wallace test was used, followed by Bonferroni correction for *post hoc* analysis. Separate sensitivity tests were performed for non-parametric datasets after log transformation and results were similar to those from non-parametric tests prior todata transformation.